

## ABSTRACT

Title of Document: APPLICATION OF EJECTOR CYCLE ON HOUSEHOLD REFRIGERATORS

Manjie Li, Master of Science, 2015

Directed By: Research Professor Yunho Hwang, Ph.D.  
Department of Mechanical Engineering

In this study, an enhanced single-evaporator refrigeration system with an ejector was studied, which can recover part of the expansion loss from the system. The focus of the study was applying the ejector cycle to the household refrigerator experimentally and numerically, which had a small refrigerant mass flow rate and a sub-zero evaporating temperature. The ejector designed from the previous work was fabricated and its test facility was constructed and instrumented. The test results were analyzed with the partial help of simulation software. The achieved maximum COP of ejector cycle was 2.4 at evaporating temperature of  $-10^{\circ}\text{C}$ . Test results show that the pressure drop along the ejector suction loop needs to be carefully designed and poor mixing inside the ejector significantly impairs the ejector and overall system performance. More research work is needed to further prove the potential of ejector cycle in refrigerator system.

APPLICATION OF EJECTOR CYCLE ON HOUSEHOLD REFRIGERATORS

By

Manjie Li

Thesis submitted to the Faculty of the Graduate School of the  
University of Maryland, College Park, in partial fulfillment  
of the requirements for the degree of  
Master of Science  
2015

Advisory Committee:  
Research Professor Yunho Hwang, Chair  
Professor Jungho Kim  
Associate Professor Bao Yang

© Copyright by

Manjie Li

2015

## **Dedication**

To My Parents

## **Acknowledgements**

For all the past twenty four years, life has given me so many precious and worthy moments which I shall memorize forever, and the part with CEEE, University of Maryland is the most special experience that made me who I am and led me to where I should be. Therefore, I would like to express my deepest gratitude to all those people who helped me, guided me and accompanied me in my journey of research.

First, I will give my special gratitude to my advisor, Dr. Yunho Hwang, without whom I would never make this achievement. His patient guide and rich experience helped me become an eligible engineer and researcher. And his passion and insistence of research influenced me deeply. I would also like to express my thanks to Dr. Radermacher, for all the support and help throughout my research and career.

In addition, I would personally give my appreciation to Mr. Jan Muehlbauer, who gave me so many valuable advices and experiences for my research and life in US. I would also extend my gratitude to Dr. Hoseong Lee, Sahil Popli, Bracha Mandel, Suxin Qian, Tao Cao, Xiaojie Lin, Zhiwei Huang, Zhilu Zhang, Andrew Rivera, and all people in the CEEE who made this journey unforgettable.

My last thanks goes to my parents, whose lasting support gave me continuing encourage to walk through all those long and challenging time.

Although my journey with the CEEE is going to end, its impacts will always be with me and guide me towards the future. And the future is just about to start.

## Table of Contents

Dedication .....	ii
Acknowledgements .....	iii
List of Tables .....	vii
List of Figures .....	viii
Nomenclature .....	xi
1. Introduction .....	1
1.1 Background .....	1
1.2 Objective .....	5
2. Literature Review .....	6
2.1 Introduction of Ejector Cycle in the Vapor Compression System .....	6
2.2 Development of Ejector Model .....	10
2.3 System Performance in Ejector-Expansion Refrigeration Cycle (EERC) .....	16
2.4 Application of EERC to Multiple Evaporator Refrigeration Systems .....	21
2.5 Low GWP Refrigerants .....	23
3. Test Facility .....	27
3.1 Ejector Design .....	27
3.1.1 Motive Nozzle Block .....	29
3.1.2 Suction Chamber Block .....	31
3.1.3 Mixing and Diffuser Block .....	32

3.1.4 Alignment Piece of the Needle .....	33
3.1.5 Assembly of Ejector .....	34
3.2 Ejector Fabrication .....	34
3.3 Compressor.....	36
3.4 Condenser and Condenser Fan.....	37
3.5 Electric Expansion Valve .....	38
3.6 Heaters.....	38
3.7 Flash Tank.....	39
3.8 Test Facility Design .....	40
3.8 Test Facility Construction.....	46
3.9 Instrumentation.....	49
3.9.1 Thermocouples and Pressure Transducers .....	49
3.9.2 Mass flow meters.....	51
3.10 Test Conditions .....	52
3.11 Data Reduction.....	53
3.12 Uncertainty Analysis .....	57
4. Test Results and Data Analysis .....	58
4.1 Baseline VCC Tests Results.....	58
4.2 Energy Balance Analysis .....	61
4.3 Ejector-Expansion Refrigeration Cycle Test Results.....	67

4.4 Summary of Experimental Results.....	77
5. Thermodynamic Modeling of Ejector-Expansion Refrigeration Cycle .....	80
5.1 Cycle Modeling.....	80
5.2 Modeling Results.....	81
5.3 Model Validation.....	84
5.4 Discussion .....	88
6. Conclusions .....	91
7. Future Work.....	93
Reference .....	94

## List of Tables

Table 2-1: Values of GWP and ODP for Refrigerant Used in Refrigeration System [31] [32] .....	24
Table 2-2: Comparison of Different Refrigerants with -15/30°C Condition [32] .....	25
Table 3-1: Optimized Non-Dimensional Values of the Designed Variables.....	28
Table 3-2: Non-Dimension Values of the Other Ejector Geometries.....	29
Table 3-3: Specifications of Instruments .....	52
Table 4-1: Summary of Baseline Test Results at (-10°C) Evaporating Temperature .....	59
Table 4-2: Summary of Baseline Test Results at (-28°C) Evaporating Temperature .....	60
Table 4-3: Parameters and Assumptions used in Energy Evaluation .....	64
Table 4-4: Summary of Heat Gain Calculation .....	65
Table 4-5: System Level Energy Balance Evaluation for Baseline Test .....	66
Table 4-6 Energy Balance before and after Heat Gain Correction.....	67
Table 4-7: Summary of EERC Test Results at -10°C Evaporating Temperature.....	70
Table 4-8: Comparison of Test Results between VCC and EERC.....	71
Table 4-9: Evaluation of Sudden Expansion and Sudden Contraction.....	73
Table 4-10: Pressure Lift Estimation under Designed Efficiencies.....	74
Table 5-1: Simulation Results of EERC under -10°C Evaporating Temperature .....	82
Table 5-2: Comparison of Model Results and Test Results .....	85

## List of Figures

Figure 1-1: Energy Flow Chart of US in 2013 [1].....	1
Figure 1-2: Projection of Extraction Remaining Years of Fossil Fuel [2].....	2
Figure 1-3: Average Residential Energy Consumption by End-use [3] .....	3
Figure 1-4: Electricity Consumption by End-use for All Commercial Building [4] .....	4
Figure 2-1: Working Principle of Single-Phase Ejector [5].....	7
Figure 2-2: Schematic Diagrams of Conventional VCC and EERC [6].....	9
Figure 2-3: Comparison between Constant Pressure Ejector (left) and Constant Area Ejector (right) [5] .....	10
Figure 2-4: Ejector Model Developed by Huang et al. [8] .....	11
Figure 2-5: Mixing Model of Constant Area Ejector by Yapici and Ersoy [5] .....	12
Figure 2-6: Optimum Design Curve for R-123 at Different Operating Conditions [5]....	13
Figure 2-7: Wall Static Pressure Distribution along the Ejector [12].....	14
Figure 2-8: Variation of Mach Number and Static Pressure inside Steam Ejector [13]...	16
Figure 2-9: Test Schematic of Menegay and Kornhauser’s Test [20].....	18
Figure 2-10: Improved Transcritical CO <sub>2</sub> Ejector Cycle by Li and Groll [24].....	19
Figure 2-11: Pressure Profile of Two-phase Ejector with Different Mixing Section Length [26].....	20
Figure 2-12: Novel Multi-evaporator System Proposed by L. Kairouani [27].....	22
Figure 2-13: Three Cycle Configurations of Ejector Cycle in Multi-Evaporator Systems [28].....	22
Figure 2-14: Modified Dual-evaporator Ejector System for Transcritical CO <sub>2</sub> Cycle [29] .....	23

Figure 2-15: Dual-nozzle Design from Lin et al. [30] .....	23
Figure 2-16: Comparison of COP and GWP among Refrigerants.....	26
Figure 3-1: Geometry of Designed Ejector (a) Ejector Inner Structure; (b) Motive Nozzle Structure .....	28
Figure 3-2: 3D Drawing of Designed Motive Nozzle Block.....	30
Figure 3-3: 3D Drawing of the Suction Chamber Block .....	31
Figure 3-4: 3D Drawing of the Mixing and Diffuser Block .....	33
Figure 3-5: 3D Drawing of Needle Alignment Piece .....	33
Figure 3-6: Assembly Drawing of Designed Ejector.....	34
Figure 3-7: Main Parts of Manufactured Ejector (a): assembly; (b): motive nozzle block; (c): suction chamber block; (d): mixing and diffuser block) .....	35
Figure 3-8: Needle Connected to the Metering Valve .....	35
Figure 3-9: Ejector Assembly with Needle Control .....	36
Figure 3-10: Variable Speed Compressor for R600a System.....	37
Figure 3-11: Components and Housing of the Condensing Unit.....	37
Figure 3-12: Electronic Expansion Device from Sporlan [35] .....	38
Figure 3-13: Pictures of the Evaporator Heaters.....	39
Figure 3-14: Schematic of the Stainless Steel Flash Tank.....	40
Figure 3-15: Schematic of the Initial System Configurations with Two Operational Modes: (a) Baseline (b) EERC .....	42
Figure 3-16: Modified Schematic of Ejector System in (a) Baseline VCC and (b) EERC .....	43
Figure 3-17: Electrical Schematic.....	45

Figure 3-18: Overview of Bottom Level Test Facility .....	47
Figure 3-19: Upper Level Test Facility .....	47
Figure 3-20: Electric Box Overview.....	48
Figure 3-21: Data Acquisition System Setup.....	49
Figure 3-22: Surface (left) and In-steam (right) T-type Thermocouples .....	50
Figure 3-23: Setra AccuSense High Accuracy Pressure Transducers. ....	50
Figure 3-24: Bronkhorst Mini CORI-FLOW Meters.....	51
Figure 3-25: Simplified Schematic and P-h Diagram of EERC .....	55
Figure 4-1: Percentage of Energy Balance Deviation for Evaporator under Various Conditions .....	62
Figure 4-2: Dimensions of Insulated Tubes .....	63
Figure 4-3: P-h Diagrams of Baseline VCC and EERC .....	69
Figure 4-4: System COP under Different Compressor Frequencies.....	75
Figure 4-5: Flow Rates and Entrainment Ratio under Different Compressor Frequencies .....	76
Figure 4-6: Ejector Pressure Lift under Different Compressor Frequencies .....	77
Figure 5-1: Parametric Study of Compressor Suction Pressure.....	83
Figure 5-2: Parametric Study of Ejector Nozzle Exit Pressure.....	83
Figure 5-3 Comparison of P-h diagram between Modeling Results and Test Results .....	87
Figure 5-4: Sensitivity Study of Ejector Efficiencies .....	90

## **Nomenclature**

A	Area
D	Hydraulic Diameter
j	Data Point Index
k	Conductivity
$\dot{m}$	Mass Flow Rate
N	Number of Data Points in the Collected Data Set
h	Enthalpy
P	Pressure
Q	Heat
Re	Reynolds Number
s	Entropy
U	Heat Transfer Coefficient
u	Velocity
w	Entrainment Ratio
W	Work
x	Quality
$x_j$	Measured Variable Data Point at Index j

$\bar{x}$  Average of the Measured Variable over the Entire Data Set

$\eta$  Efficiency

$\varepsilon$  Uncertainty

$\rho$  Density

$\mu$  Dynamic Viscosity

*Subscript*

1, 2, 3, 4 ... Refrigerant States

4s, 6s, 10s Refrigerant States after Isentropic Process

C Cooling

d Diffuser

m Mixing

mn Motive Nozzle

mf Motive Flow

p Pipe

ref Refrigerant

sn Suction Nozzle

sf Suction Flow

sys System

*Abbreviation*

CAD Computer Aided Design

COP Coefficient of Performance

CFD Computational Fluid Dynamics

EES Engineering Equation Solver

EEV Electronic Expansion Valve

EERC Ejector-Expansion Refrigeration Cycle

GWP Global Warming Potential

NPT National Pipe Thread

ODP Ozone Depletion Potential

STD Standard Deviation

VCC Vapor Compression Cycle

# 1. Introduction

## 1.1 Background

After age of electricity, the structure of energy utilization largely changed. Electricity, as an efficient carrier of energy, has become a major energy source for residential and commercial equipment and appliances. Figure 1-1 shows the energy flow chart for U.S. in 2013. From the energy flow chart, total primary energy used for electricity generation was 38.2%, while the efficiency of electricity generation was only 32% [1]. Therefore, two-third of primary energy was transferred to heat during the electricity generation. This also means if 1 kWh electricity can be saved from end-users, 3 kWh energy can be saved from the primary energy.

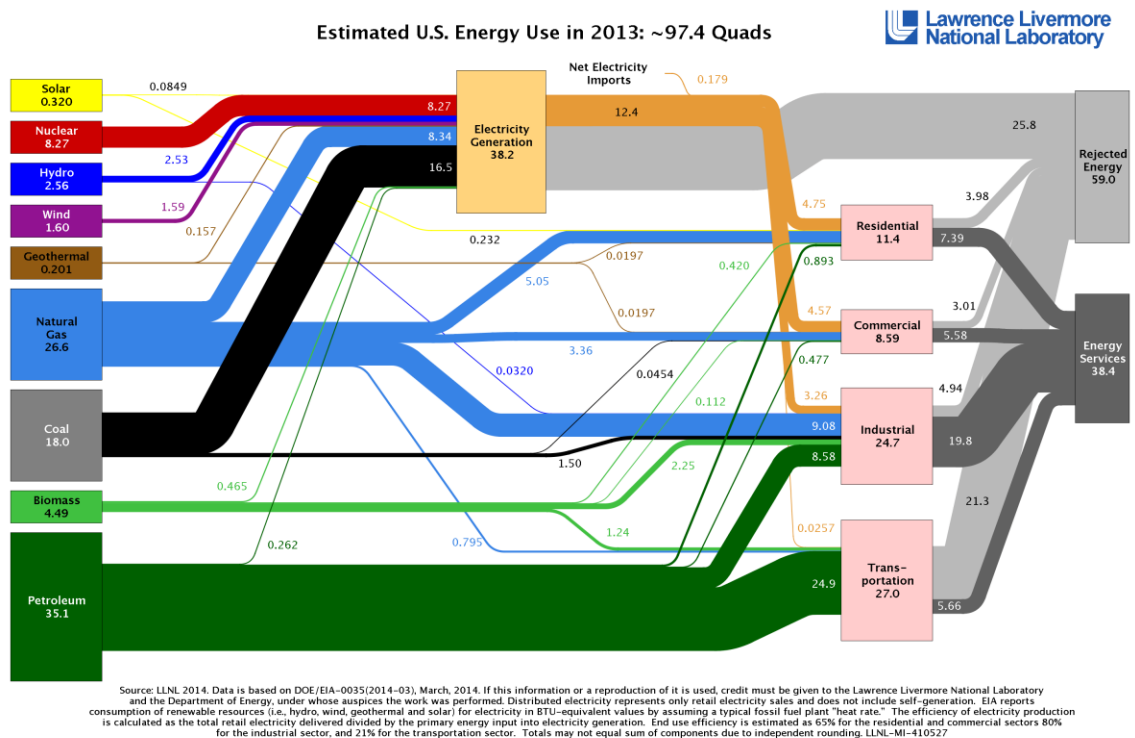
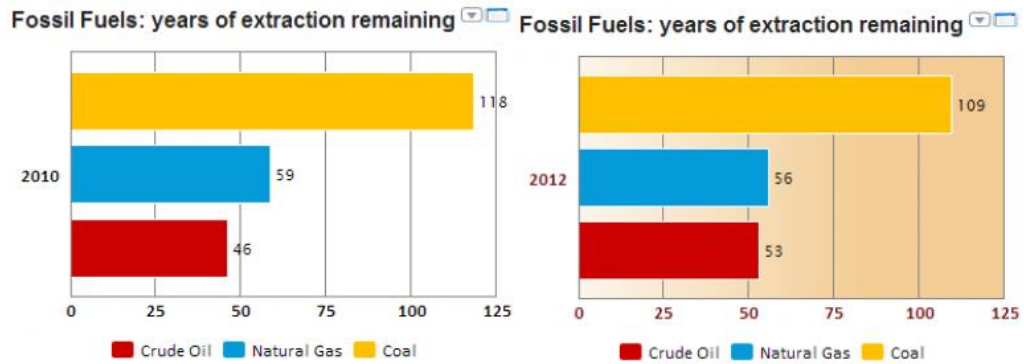


Figure 1-1: Energy Flow Chart of US in 2013 [1]

As shown in Figure 1-1, fossil fuels (coal, natural gas, petroleum) takes 82% of primary energy. However, the amount of fossil fuel is limited and the remaining is decreasing.

From statistical review on world energy by BP in 2013, the projection of remaining extraction years of coal and natural gas is decreasing from 2010 to 2012 as shown in Figure 1-2.



**Figure 1-2: Projection of Extraction Remaining Years of Fossil Fuel [2]**

While fossil fuel production is projected to decline, the world energy demand is still increasing so that the energy supply will not meet the demand soon or later unless alternative energy is well developed. Therefore, a stable energy supply is an urgent problem that whole human kinds are facing.

Whereas, energy saving could partially help solve this issue. What can we do to save energy? There are several solutions for this challenge. One way is through the improvement of electricity generation efficiency. Another way is to have alternative energy. Although these two options are economically feasible, it would take long time depending on the technology. The most realistic option that could be realized within a shorter time frame is saving electricity from the end use.

Where is the electricity used for? Again the answer can be found in Figure 1-1, about 1/3 was used for residential use, 1/3 for commercial use and the last 1/3 for industrial use.

From the latest residential energy consumption survey by the EIA in 2009 (Figure 1-3),

most of electricity, about 59%, was used for heating purpose. Although refrigerator itself doesn't utilize high power consumption, it is operating all the time so that it takes about 5% of the total energy consumption.

Average Residential Energy Consumption by End-use (2009)

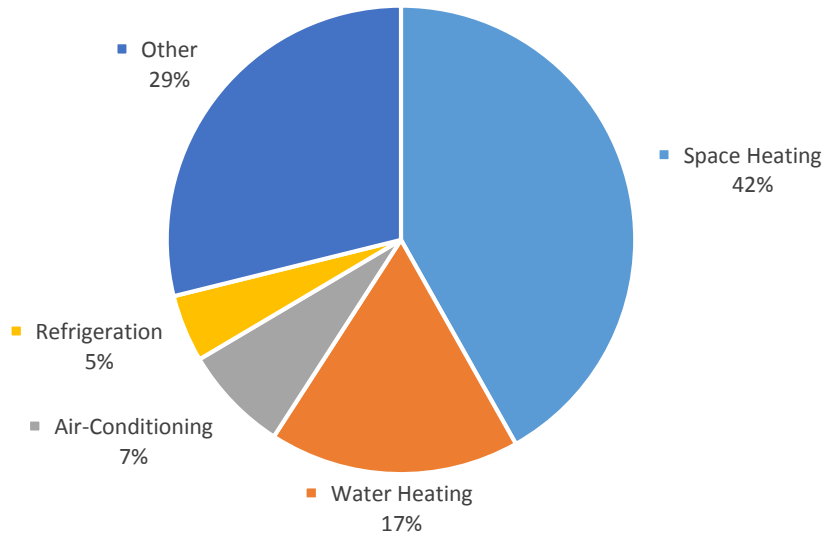


**Figure 1-3: Average Residential Energy Consumption by End-use [3]**

Figure 1-4 shows the latest energy consumption data for all type commercial buildings in 2003. Different from the residential use, lighting takes the most of electricity consumption, and heating and cooling also take a large portion. This survey contains all types of buildings including supermarket, grocery store and convenience store, which consume large energy for refrigeration. Moreover, the energy consumption for refrigeration is almost the same amount used for space cooling. However, for industrial use, there is no existing detailed information on electricity use, so this part is not included in the following analysis.

### Total Commercial Building Electricity Consumption by End-use for All Buildings (2003)

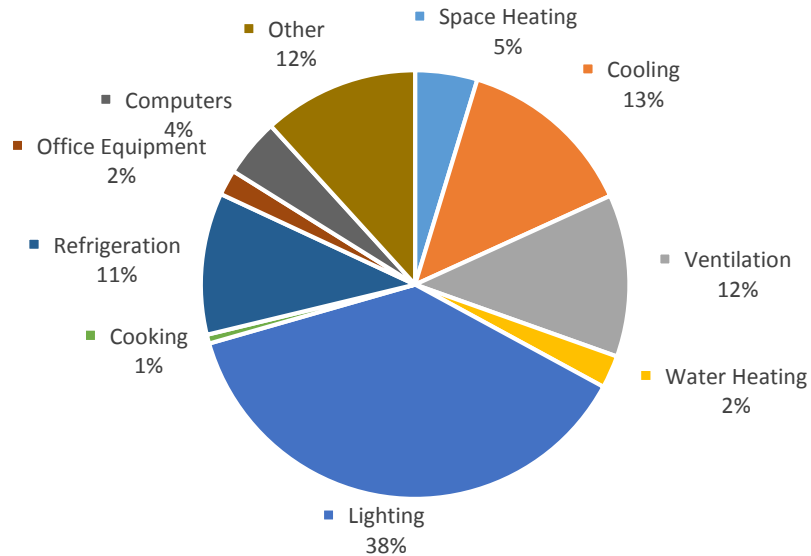


**Figure 1-4: Electricity Consumption by End-use for All Commercial Building [4]**

If it is assumed that the fraction of electricity use for residential and commercial keep the same along the years, it can be estimated that about 17.9% of residential and commercial electricity use is responsible for cooling purpose (refrigeration and air-conditioning), and refrigeration is 7.9%. If the coefficient of performance (COP) of the vapor compression cycle increases about 10%, there is around 2% electricity that can be saved from the residential and commercial cooling energy use. Although this 2% is a small number, this small step could contribute to the energy saving.

Among the researches for improving the vapor compression cycle efficiency, the ejector expansion refrigeration cycle (EERC) is one of the promising technologies for which lots of researchers are working on. It was already proven that the EERC could achieve a COP improvement around 10% under certain applications such as air conditioning.

## **1.2 Objective**

This study is intended to investigate the performance of ejector refrigeration cycle under a medium temperature refrigeration condition. The objectives of this study are approached in two research aspects: one is experimental research, and another is modeling research.

Experimental research aspects are as follows:

- Design and fabricate the prototype of ejector for medium temperature refrigeration application
- Design and construct the test facility to test both the basic vapor compression cycle and EERC
- Experimentally evaluate both the vapor compression cycle and EERC under various operating conditions

Modeling research aspects are as follows:

- Simulate the performance of the basic vapor compression cycle and EERC under various operating conditions
- Compare and analyze simulation results with experiment results
- Conduct parametric study for design and operating parameters of the ejector to explore the future development direction for the ejector refrigeration cycle

## **2. Literature Review**

### **2.1 Introduction of Ejector Cycle in the Vapor Compression System**

An ejector, also known as a jet or an injector in some literature, is a device of using high pressure fluid to compress low pressure fluid, and has the potential to recover expansion loss from high pressure fluid. Since there is no moving part, it is noise-free and reliable, and has long lifetime and low initial and running cost. Also, the use of the ejector in the vapor compression cycle can save high grade energy source such as electricity. These advantages make an ejector a perfect candidate for improving conventional vapor compression system.

There are two main ways for applying the ejector. One is using vapor phase refrigerant, which is generated by heat source to pump the low pressure fluid. In this application, the heat can be sustainable energy such as solar energy or waste heat. Thus, it provides a very potential way in utilizing low grade heat. Figure 2-1 shows such an example. In this cycle, the ejector and pump fully replace the compressor so that this type of cycle is also named as heat-driven refrigeration system. Since all flows inside the ejector are in vapor phase, this ejector is also called as “single-phase ejector.”

Figure 2-1 shows the working principle of the single phase ejector. It shows the high pressure saturated vapor (state 0) and the low pressure saturated vapor (state 7). In the ejector, the motive flow (state 0) is first accelerated with a convergent-divergent nozzle to generate a pressure lower than the suction flow (state 7). With this low pressure, the suction flow is sucked into the mixing chamber. The two flows fully mixes with each other, and then are compressed by the diffuser to reach an intermediate pressure. At the exit of the ejector, the refrigerant state is still in vapor phase. Since in a single-phase

ejector, the whole process is closer to an isentropic process, the refrigerant at ejector outlet (state 4) can be superheated vapor if the suction flow (state 7) has some degrees of superheat. The refrigerant discharged from the ejector (state 4) then enters the condenser to exchange the heat with environment and reaches to a saturated liquid condition. The liquid refrigerant at the condenser outlet (state 5) is then separated into two parts. One is sent to the liquid pump, pumped to high pressure same with that of state 0, and absorbs heat from any heat source provided to the generator. After the generator, the refrigerant flows back to the motive flow (state 0). Another part of flow from the condenser (state 5) is sent to the expansion valve, reduced to lower pressure (state 6) and produces the cooling effect. At the exit of the evaporator, the refrigerant (state 7) flows back to the ejector suction.

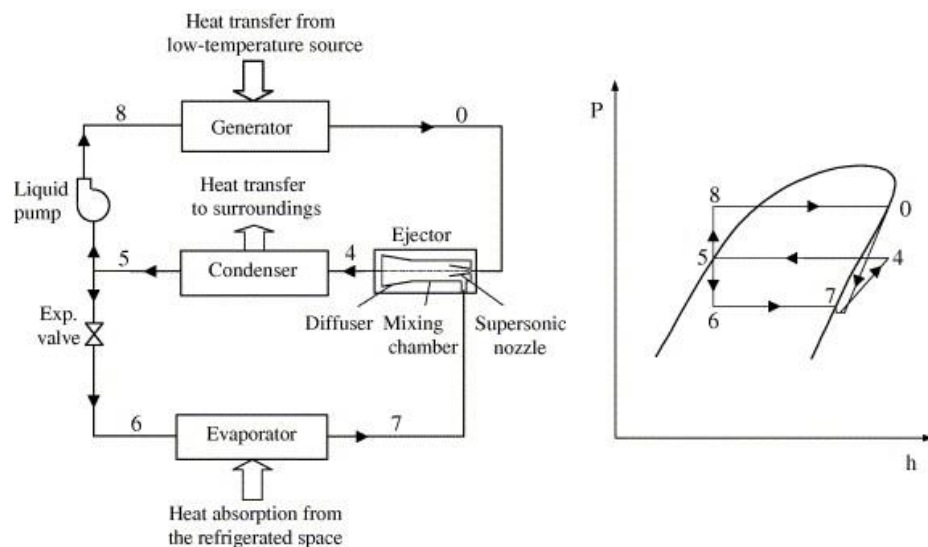


**Figure 2-1: Working Principle of Single-Phase Ejector [5]**

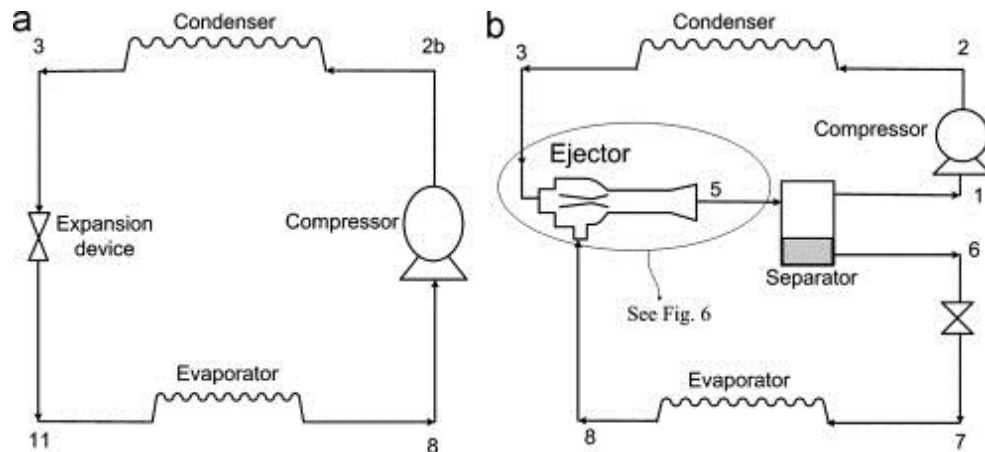
The main advantages of this cycle are in two folds: (1) there is no moving part in the system except the liquid pump and (2) the low grade heat can be used to partially drive

the whole refrigeration system. The challenges for this application are a low coefficient of performance (COP) and the inflexible operation conditions for the ejector.

The second application is to use the ejector as an expansion device to recover throttling loss in a typical vapor compression cycle (VCC). As known, one of the big energy losses in the conventional VCC is throttling loss. For typical VCC, a high pressure liquid refrigerant is expanded to low pressure two-phase refrigerant. Although an ideal expansion process is isentropic and produces work, the actual expansion process is isenthalpic so that the energy difference between these two processes is lost. This loss can be relatively larger for some refrigerants such as R-502 and R-744 than others. Although it is hard to recover all of the energy loss in this process, there is a great potential to recover. The closer the efficiency of the ejector to be 1, the more energy can be recovered.

Figure 2-2 shows the comparison of the conventional VCC and the ejector-expansion refrigeration cycle (EERC). In an EERC, a saturated liquid (state 3) from the condenser works as the motive flow for the ejector instead of the typical expansion device. This motive flow is expanded first to a low pressure and mixed with the saturated vapor from the evaporator. The ejector exit flow (state 5) is in two-phase, and this two-phase flow is separated to vapor phase and liquid phase at the separator. The saturated vapor after the separator is then supplied to the compressor, compressed to the high pressure level and exchanges heat with environment in the condenser. The saturated liquid exiting the separator is directed to the expansion device, expanded to lower pressure and produces the cooling effect.

The EERC is separated into two parts: high pressure part and low pressure part. The intersection of these two parts is the ejector and separator. In the EERC, there is energy saving from the compressor because the compressor suction pressure (state 1) is higher than that (state 8) of conventional cycle in addition to the energy saved by recovering the throttling loss.



(a) Conventional VCC (b) EERC

**Figure 2-2: Schematic Diagrams of Conventional VCC and EERC [6]**

Different from heat-driven refrigeration system, the system COP of the EERC is higher than the basic VCC. The EERC cycle can improve the COP by 10-20% in average [6]. For the modeling of the process through an ejector, there are mainly two approaches depending upon the geometry of the mixing section: constant pressure mixing and constant area mixing [8], as shown in Figure 2-3. In the ejector with a converged section after the motive nozzle, the constant pressure model is used for mixing process so that it is assumed that two flows are mixed at a constant pressure. After the mixing, the mixture passes through the constant area section for further mixing. For a constant area ejector, there is no convergent section before the constant area section. Therefore, two flows are not mixed at the inlet of the mixing chamber.

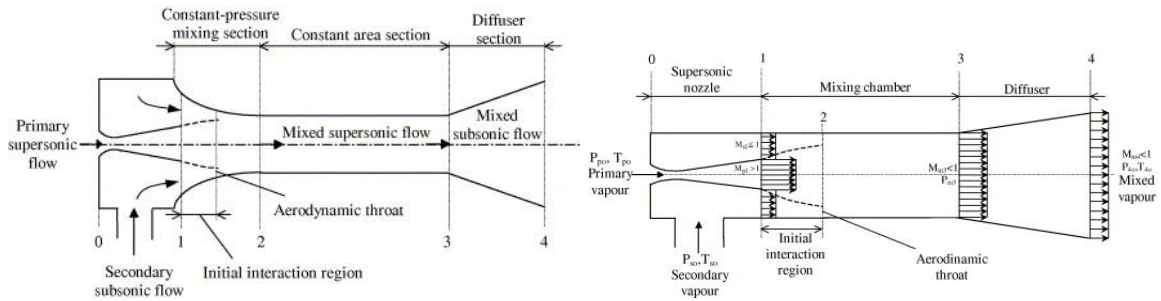


**Figure 2-3: Comparison between Constant Pressure Ejector (left) and Constant Area Ejector (right) [5]**

Keenan [7] and Huang et al. [8] concluded that the constant pressure ejector has a better performance. However, Yacipi and Ersoy [5] later concluded that the constant area ejector yielded a better COP improvement in EERC at the same operating temperature.

For the 1-D thermodynamic ejector model, researchers prefer to assume a constant pressure mixing for the simplicity no matter it is constant pressure ejector or constant area ejector.

## 2.2 Development of Ejector Model

The concept of ejector has been first introduced to the refrigeration system as a heat-driven cycle in 1901 by Le Blanc and Parsons. Since then, the advantages of the ejector refrigeration cycle have enjoyed the popularity among researchers. As the key part of the system, the modeling of the ejector is the most important topic but also very challenging. The development of the single phase ejector is simpler than two-phase ejector so that most of the successful studies were conducted for the single-phase ejector.

In 1942, Keenan and Neumann [7] developed a series of 1-D continuity, momentum and energy equations to predict the ejector performance. However, it did not provide

information on the choking phenomena. Then further study was focused on the irreversibility. Sun et al. [9] modified Keenan's model and introduced isentropic efficiencies to consider friction losses. They assumed that the mixing of the two streams was complete before a normal shock wave could occur at the end of the mixing chamber. The isentropic efficiencies were set at constant values, which was the simplest way to consider irreversibility. It was found that the choking of the suction flow in the mixing chamber plays an important role. To consider the choking of the suction flow, Huang et al. [8] suggested separating different performances of ejector. In their analysis, it was assumed that there was a hypothetical throat inside constant area section, not in the constant pressure mixing chamber as shown in Figure 2-4 at y-y position, and energy conservation and gas dynamic equations were used in the model. Huang summarized three modes that the ejector may work at and also suggested the ejector working at double-choking mode because it has a larger entrainment ratio. Huang also developed a more complicated model considering the shock and the model agreed with experiment data very well.

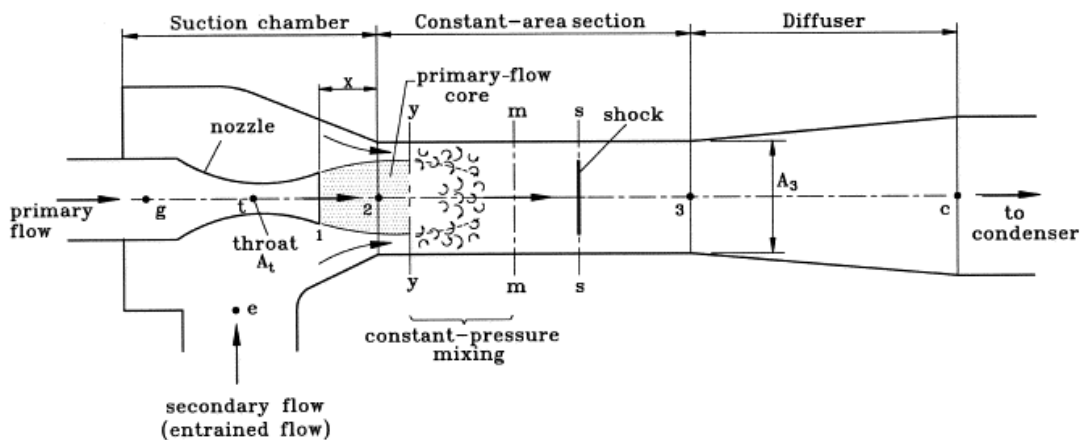


**Figure 2-4: Ejector Model Developed by Huang et al. [8]**

The ejector researchers in their early stage were focusing on constant pressure ejector. Yapici and Ersoy [5] developed constant-area model and reported that constant area ejector has a better performance in refrigeration system at the same operating conditions. Yapici and Ersoy [5] first developed a model for constant area ejector with different pressure and Mach number for two flows at the inlet of constant area section. Since the motive flow velocity is higher than the suction flow, the motive vapor expands against the suction vapor, and then the motive stream behaves as a nozzle for the suction stream and causes the hypothetical throat. The velocity of the suction flow can reach supersonic at this hypothetical throat. The special approach was made for the mixing section simulation differently from others, which assumed the inlet condition of constant area was already well mixed. Figure 2-5 shows the control volume used.

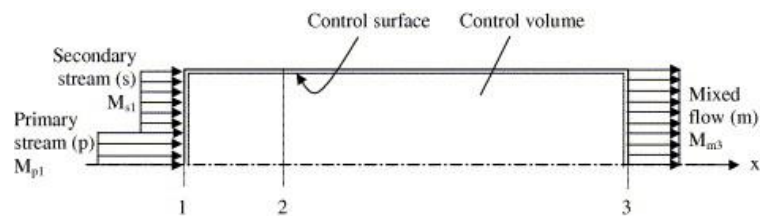


**Figure 2-5: Mixing Model of Constant Area Ejector by Yapici and Ersoy [5]**

Although the analysis was done for the single phase ejector, this model was also applied to the two-phase ejector. However, two-phase ejector also needs to consider the expansion of liquid and phase changing phenomena, which is much more complicated. Yapici and Ersoy claimed that there exists an optimum design trend for area ratio at different operating conditions as shown in Figure 2-6. This research was done for the heat-driven cycle but the generation temperature could be viewed as a condensing temperature in the EERC.

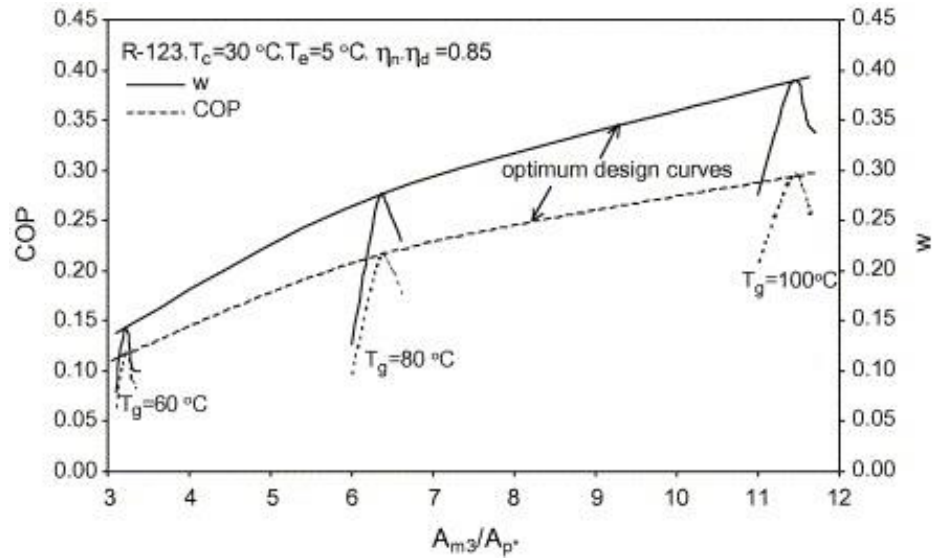


**Figure 2-6: Optimum Design Curve for R-123 at Different Operating Conditions [5]**

The inlet flows of the single phase ejector are usually superheated or saturated vapor.

However, even in heat-driven system, if the fluid mixture entering the diffuser is supersonic, it is more likely to undergo a condensation shock. This means even in heat-driven system, the study of two-phase ejector is very necessary. Sherif et al. [10] derived an isentropic homogeneous expansion/compression model considering phase change. In the model, the motive flow was a two-phase mixture while the suction flow was sub-cooled or saturated liquid. In motive nozzle, Sherif et al. separated the nozzle into convergent part and divergent part. By assuming pressure at the throat and knowing quality at the inlet, the quality at the throat could be calculated iteratively by using continuity, momentum, energy and state equations. And the same process can be used in divergent section.

Due to the complexity in modeling the flow completely, most models used 1-D thermodynamic steady state explicit equations to obtain operation parameters. However, detailed information such as shock interactions and turbulent mixing could not be

obtained this way [11]. Thanks to the latest developing in CFD software, these challenges were partially addressed by applying the CFD simulations to solve some partial implicit differential equations.

Sriveerakul et al. [12] made detailed comparison between experiment and simulation results using Fluent. Realizable k-epsilon turbulent model was used to yield a pretty good convergent performance. Comparison of static pressure inside an ejector is shown in Figure 2-7. Overall, the CFD model results in a pretty good accuracy. The effect of operating conditions and geometries were also studied and compared with experimental results in previous studies. The CFD results matched well with experimental data with some offset in mixing chamber.

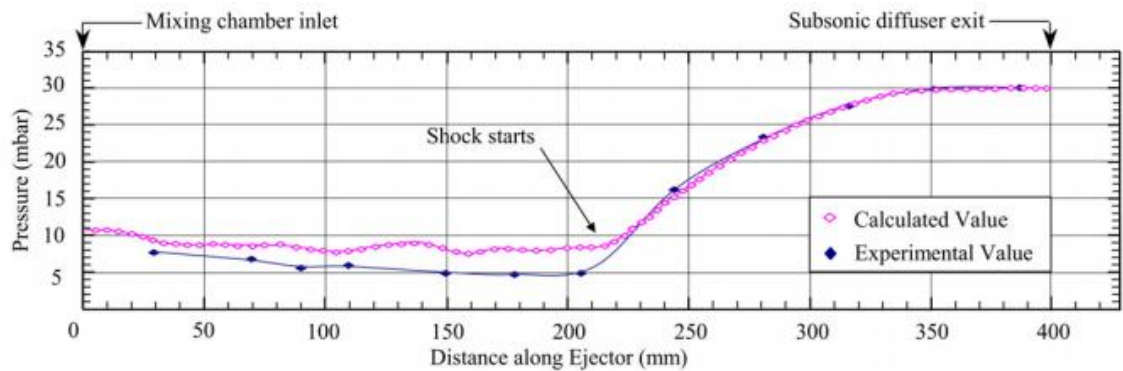
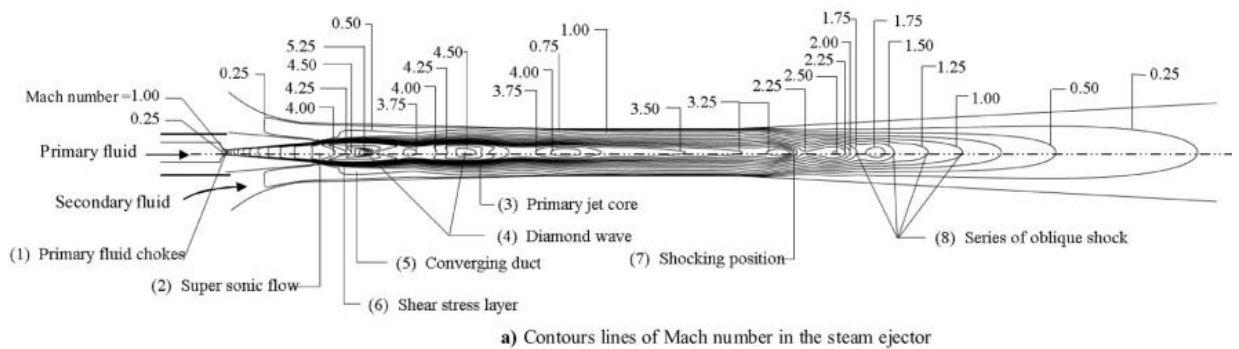


**Figure 2-7: Wall Static Pressure Distribution along the Ejector [12]**

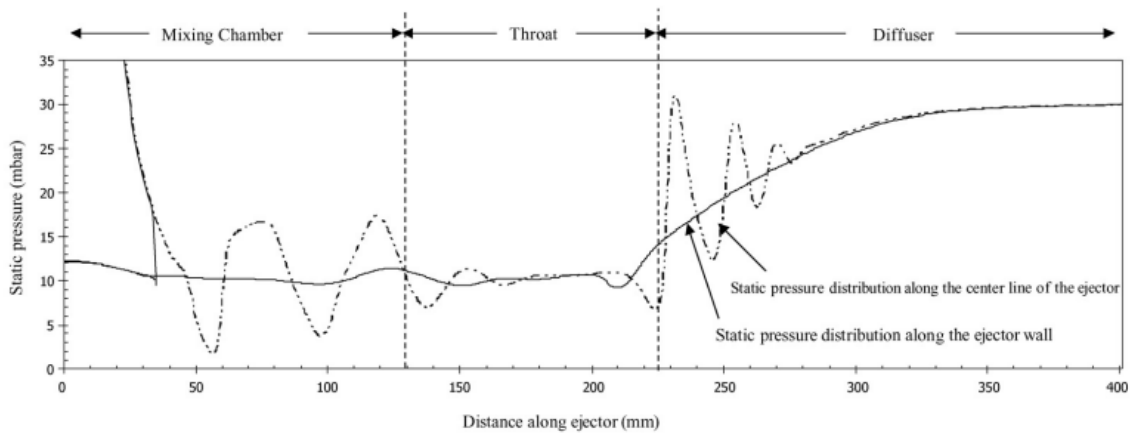
In another study, Sriveerakul et al. [13] revealed the phenomenon inside the steam ejector and analyzed the effect of operating pressures and ejector geometries with contour plots of Mach number at different locations. In Figure 2-8, CFD simulation result of choked flow mode is shown. From the change of Mach number, it was seen that the motive flow became supersonic flow after the convergent-divergent nozzle. After the nozzle, because of the great change in volume, the motive flow continued its expansion and acceleration.

To preserve the static pressure across the free boundary between this jet core and the surrounding suction flow, a series of oblique shock appears, called as “diamond wave”. This is the reason for large fluctuation in static pressure. When looking at the fluid surrounding the jet core, which mostly is the suction flow, it was found that because of the large velocity difference between two flows, the expansion of the motive flow formed a “nozzle” for the suction flow, and the suction flow reached sonic velocity in the middle of the mixing chamber. After a certain mixing, flow shock appeared.

Result of pressure effect was further investigated under different ejector back pressures. The simulation result shows a good agreement with analysis done by Huang et al. [8]. The special point of this study was that with the help of CFD simulation, more details of flow interaction could be revealed. With this information, which 1-D thermodynamic model cannot show, the optimization of ejector design can be conducted.



a) Contours lines of Mach number in the steam ejector



b) Static pressure distribution of the steam ejector

**Figure 2-8: Variation of Mach Number and Static Pressure inside Steam Ejector [13]**

Real refrigerant, R-142b, was used in CFD simulation by Bartosiewicz et al. [14]. The author concluded that CFD simulation could provide useful information inside the supersonic ejector and it was essential to understand the physics inside. It is worth noting that Bartosiewicz et al. found out that the choice of an appropriate turbulence model was crucial.

### 2.3 System Performance in Ejector-Expansion Refrigeration Cycle (EERC)

The early research of ejector refrigeration system was only focused on heat-driven application. In 1990, Kornhauser [15] first used an ejector as an expansion device to

reduce throttling loss in the VCC and tried to develop a numerical model to calculate the states inside ejector. 1-D thermodynamic model was developed and iteratively calculated the state points inside ejector by assuming the mixing pressure. Eight different refrigerants were evaluated on the potential of system where the ejector worked as an expansion device. It was found that refrigerants with more energy loss in throttling process have more potential in improving system COP. The improvement of COP as compared with the conventional cycle was around 12% - 30%.

Nehdi et al. (2006) [16], Bilir and Ersoy (2008) [17] and Sarkar (2010) [18] kept the assumption that two flows mixed at the same pressure. Bilir and Ersoy's 1-D model is a little bit different from others. They assumed the pressure after mixing section rather than the pressure at which two flows started to mix. All of them investigated the effect of operating temperatures. It was concluded that EERC has a higher COP improvement when the condensing temperature increases and the evaporating temperature decreases. Nehdi et al. found that geometric design had considerable effect on the ejector performance. Bilir and Ersoy concluded that in EERC, system performance was not so sensitive to area ratio and still showed better performance at off design conditions.

Compared to the modeling work, there is less work on the experiment basis. In 1995, Harrell et al. [19] tested a two-phase ejector of R-134a, the COP improvement was in a range of 3.9% - 7.6%. This is far below the estimated COP improvement in modeling. Menegay and Kornhauser [20] also tested a similar system for R-12 and showed a 3.8% improvement in COP. During the test, Menegay and Kornhauser observed a large effect due to non-equilibrium and came up with a bubbly flow tube to minimize it. From Menegay and Kornhauser's test, it was shown that additional hot gas to the motive flow

could be an efficient way to control flow rate. Figure 2-9 shows the schematic. Pottker et al. [21] showed the ejector system with R-410A had an 8.2%-14.8% improvement as compared with the conventional VCC.

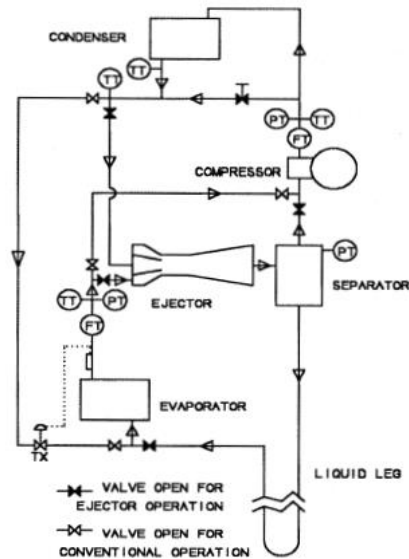


**Figure 2-9: Test Schematic of Menegay and Kornhauser’s Test [20]**

More experimental works have been conducted for improvement of initial ejector expansion system. Disawas and Wongwises [22] provided the comparison data of EERC and conventional VCC for R-134a. There was no expansion valve at the upstream of evaporator. In their system, there were two evaporators in parallel, one of which connected directly to the compressor. This configuration was well designed for air-conditioning applications, which worked for not-so-low evaporating temperature and would not work for refrigerator requiring  $-20^{\circ}\text{C}$  evaporating temperature. It was shown that the motive flow rate was more dependent on evaporating temperature than condensing temperature, which gave a good point for control and operating condition design.

Considering that the main benefit of ejector-expansion refrigeration cycle is the recovery of throttling loss, more system improvement would be achieved for refrigerants with large throttling losses, which are largely dependent on the thermophysical properties of refrigerant. That is also the reason why R-744 ejector cycle is extremely attractive in this area. Liu et al. [23] first evaluated transcritical CO<sub>2</sub> cycle with the same system layout as that for other refrigerants. However, this type of system showed constraints between the entrainment ratio of the ejector and the quality of the ejector outlet stream because the ejector outlet quality ( $x$ ) has to satisfy the condition of  $x=1/(1+w)$  in steady state operation, in which  $w$  is the entrainment ratio. Li and Groll [24] proposed a new layout as shown in Figure 2-10. Since the vapor refrigerant from the separator (point 4) is at saturated vapor condition, part of the saturated vapor is directed to the evaporator to regulate the vapor quality provided to the evaporator. Elbel and Hrnjak [25] investigated the effect of internal heat exchanger in CO<sub>2</sub> ejector cycle. There was improvement but less than the initial improvement utilizing ejector.

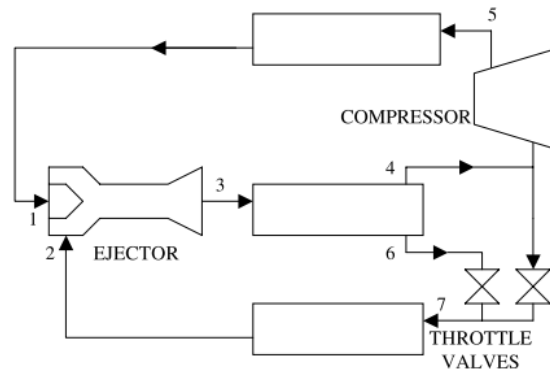


**Figure 2-10: Improved Transcritical CO<sub>2</sub> Ejector Cycle by Li and Groll [24]**

It is known that the mixing condition would significantly affect the ejector performance and the ejector efficiency. Nakagawa et al. [26] explored the effect of the mixing length

for the two-phase ejector. By showing the pressure profile along the ejector, it can be seen that an appropriate mixing length would result in a smooth pressure recovery in the diffuser as shown by the red line. If the mixing section is too short, there is not enough mixing of two flows. If the mixing section is too long, it reaches kind of “saturation point” so that there is no meaning to make the mixing section longer.

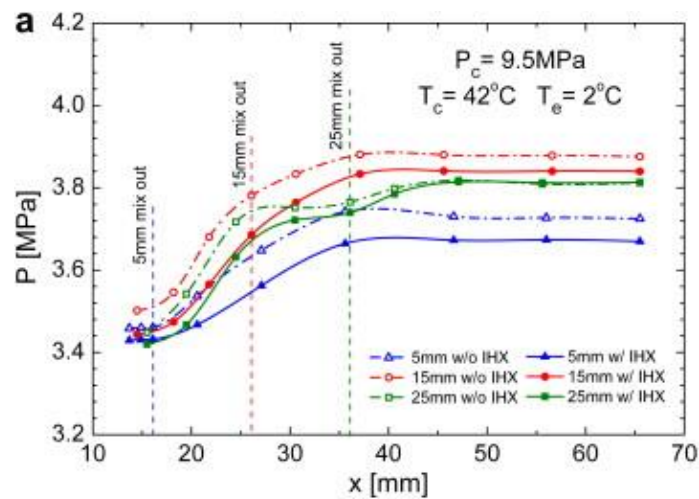


**Figure 2-11: Pressure Profile of Two-phase Ejector with Different Mixing Section Length [26]**

There are far more researches on transcritical CO<sub>2</sub> cycle using the ejector as the expansion valve, especially for the past ten years. Based on what researchers investigated for the two-phase ejector including both modeling and experiment researches, it was found that the improvement of the COP in experiment was far lower than what was expected in modeling. The reason for this could be due to the sensitivity of the ejector design. However, a more convincing reason has to be pointed out before the application of the ejector cycle in commercial refrigeration systems.

## **2.4 Application of EERC to Multiple Evaporator Refrigeration Systems**

In refrigeration applications, there are cases where multiple evaporators are needed. Conventional methods are to create parallel refrigeration loops with separate controls for temperatures. It is commonly seen that due to different requirements for various food storage, the storage temperature varies. Take household refrigerator as an example. The majority of models use only one evaporator in freezer and regulate an air damper opening to adjust fresh food cabinet temperature. Recently some models with two separate evaporators were introduced for better temperature and humidity control. These two evaporators' system could work at two different evaporating pressure levels. This pressure difference can be an additional benefit when the ejector is applied.

Kairouani et al. [27] proposed a system using two ejectors for three evaporators' system as shown in Figure 2-12. In this system, ejectors works not to recover the throttling loss, but to compress the low pressure vapor. Thus, there is less work consumed by the compressor. It is worth to note that two ejectors are operated in superheated vapor region, as a single-phase ejector, which is easier to model. However, the pressure at ejector outlet should be controlled to prevent condensation shock. The proposed system was modeled and the result showed that this improved cycle had a performance better than standard EERC system.

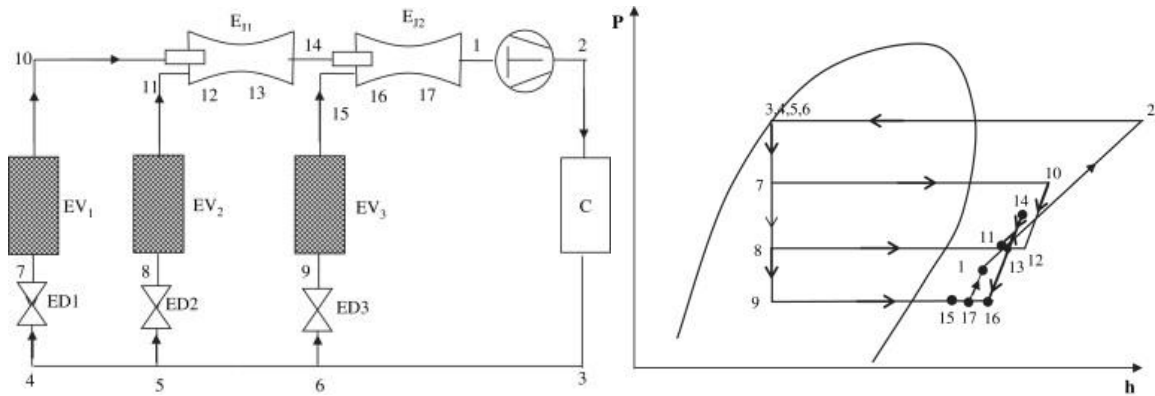


**Figure 2-12: Novel Multi-evaporator System Proposed by L. Kairouani [27]**

Liu et al. [28] continued their study on this topic and presented three cycle configurations of ejector cycle for multi-evaporator refrigeration systems. First and second loops were named as a serial system and parallel system, respectively. Liu proposed a combined system shown in the third cycle (c) in Figure 2-13. This hybrid system has two suction-line heat exchangers as regenerative heat exchanger. Liu also conducted an experimental validation of this system using R600a as refrigerant, which showed this new system had the lowest energy consumption.

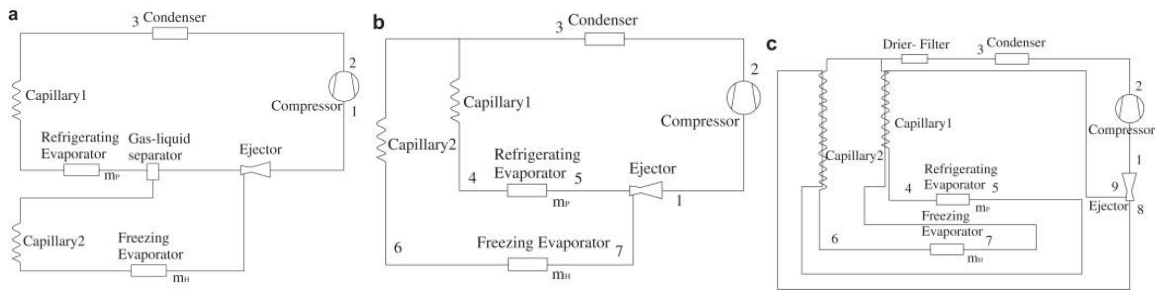


**Figure 2-13: Three Cycle Configurations of Ejector Cycle in Multi-Evaporator Systems [28]**

Bai et al. [29] presented a modified dual-evaporator ejector system based on a conventional dual-evaporator CO<sub>2</sub> cycle as shown in Figure 2-14. Two-stage ejector further increases the work recovered through an expansion process.

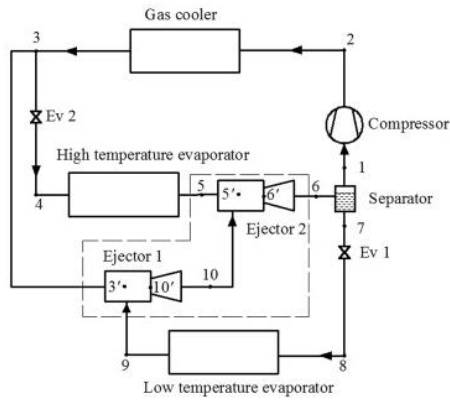


**Figure 2-14: Modified Dual-evaporator Ejector System for Transcritical CO<sub>2</sub> Cycle [29]**

Lin et al. [30] proposed an interesting ejector design with two nozzles inside the ejector. Based on this ejector, a dual-evaporator system was evaluated. This new design showed a promising system COP at range of 3 to 6.5.

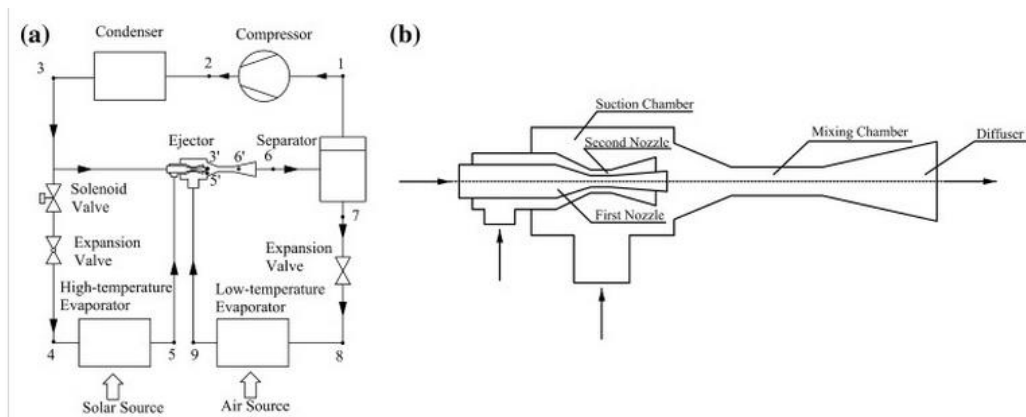


**Figure 2-15: Dual-nozzle Design from Lin et al. [30]**

## 2.5 Low GWP Refrigerants

In the present market products of commercial and household refrigerators, R-404A, R-134a and R-22 are the most commonly used refrigerant. Some old units may still use R-12 as its refrigerant but most of units now use R-134a in US market. R-404A is commonly used for commercial refrigerators in Europe. There are also units running with

other refrigerant such as R-290, R-600a, and R-32. Most of refrigerants used are non-toxic and non-flammable. However, the commonly used refrigerants have a quite high Global Warming Potential (GWP). According to Table 2-1, old refrigerant such as R-12 has an extremely high GWP and Ozone Depletion Potential (ODP). Because of its high impact on the environment, there is no unit sold with R-12 any longer. Newer refrigerants have zero ODP but some GWP. Although the GWPs of R-134a and R-404A are much lower than that of R-12, the direct emission from the refrigerant leakage from the refrigeration system cannot be ignored. Researchers are searching for new refrigerants and new systems to reduce the effect of refrigerant on the environment while providing the same system performance.

**Table 2-1: Values of GWP and ODP for Refrigerant Used in Refrigeration System [31] [32]**

Refrigerant	ODP	GWP	Refrigerant	ODP	GWP
R-11	1	4000	R-744	0	1
R-12	1	10600	R-500	0.63-0.75	6000
R-113	0.8-1.07	4200	R-501	0.53	4200
R-114	0.7-1.0	6900	R-502	0.3-0.34	5600
R-21	0.05	-	R-507	0	3800
R-22	0.055	1900	R-404a	0	3750
R-123	0.02	120	R-410a	0	1890
R-142b	0.065	2000	R-428	0	3500
R-23	0	14800	R-407a	0	1920
R-32	0	580	R-407b	0	2560
R-125	0	3200	R-407c	0	1610
R-134a	0	1600	R-417a	0	2300
R-143a	0	3900	R-422a	0	3100
R-152a	0	140	R-424	0	2400
R-1234yf	0	<4.4	R-427a	0	2100
R717	0	0	R-290	0	3.3
R-1270	0	1.8	R-600a	0	3

It is known that the refrigeration system performance is largely dependent on the refrigerant properties. Therefore, a fair comparison of different refrigerants would provide a good view of their respective achievable performance. All refrigerants are considered in the basic refrigeration system with four main components: compressor, condenser, expansion device and evaporator.

**Table 2-2: Comparison of Different Refrigerants with -15/30°C Condition [32]**

Refrigerant	$P_0$ [bar]	$P_c$ [bar]	$q_{0v}$ [kJ m <sup>-3</sup> ]	COP	$t_2$ [C]
R-717	2.36	11.67	2167.6	4.76	99.08
R-744	22.90	72.10	7979.0	2.69	69.50
R-764	0.81	4.62	818.8	4.84	96.95
R-11	0.20	1.26	204.2	5.02	42.83
R-12	1.82	7.44	1273.4	4.70	37.81
R-22	2.96	11.92	2096.9	4.66	52.95
R-32	4.88	19.28	3420.0	4.52	68.54
R-134a	1.64	7.70	1225.7	4.60	36.61
R-404a	3.61	14.28	2099.1	4.16	36.01
R-407C	2.63	13.59	1802.9	3.91	51.43
R-410A	4.80	18.89	3093.0	4.38	51.23
R-502	3.44	13.05	2079.5	4.39	37.07
R-507	3.77	14.60	2163.2	4.18	35.25
R-600a	0.89	4.05	663.8	4.71	32.66
R-290	2.92	10.79	1814.5	4.55	36.60
R-1270	3.63	13.05	2231.1	4.55	41.85

In Table 2-2, 16 refrigerants are compared.  $P_0$  is the compressor suction pressure,  $P_c$  is the compressor discharge pressure,  $q_{0v}$  is the volumetric refrigerating capacity, and  $t_2$  is the compressor discharge temperature. For some refrigerants, such as R-744, the compressor suction and discharge pressure are both high, which results in a more power consumption for the compressor, thus a lower COP. System COP also depends on the

latent capacity of the refrigerant. R-11, R-764, R-717, and R-600a have relatively higher COP than others.

To better show the comparison of COP and GWP of different refrigerants, Figure 2-16 was created based on the information in Table 2-2. The ideal refrigerant would be the one with high COP and low GWP, which means high system efficiency and low environmental impact. There are in total four refrigerants fall into this range, shown in the small diagram in Figure 2-16. All these four refrigerants can be good candidates for future refrigerants in the refrigeration system.

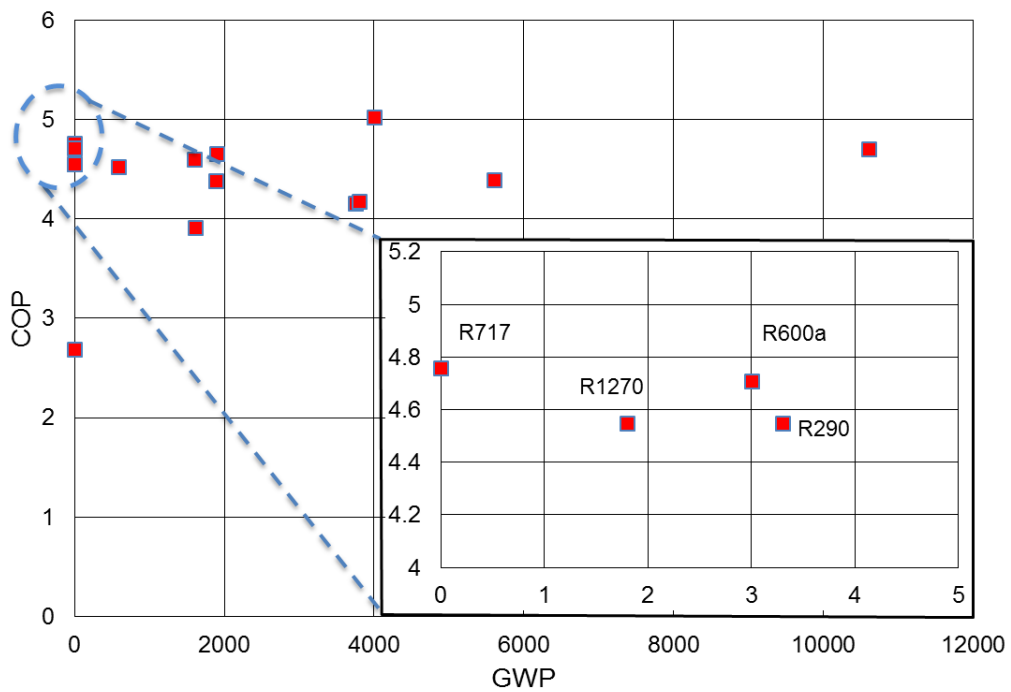


**Figure 2-16: Comparison of COP and GWP among Refrigerants**

### **3. Test Facility**

Every components have effects on other components and the system. Therefore, to ensure a good performance of designed system, key components were either designed or selected based on the system capacity. First, the ejector was carefully designed to have a reliable and sturdy structure. Then other components were selected accordingly. This chapter introduces the design of the ejector and the characteristics of other key components. System configuration is then introduced in the last several parts of this chapter.

#### **3.1 Ejector Design**

Based on the ejector design from the previous research, detailed ejector geometries were designed. In that study, five following design variables were optimized by using the parallel parameterized CFD: mixing chamber diameter, mixing chamber length, diffuser length, and motive nozzle diffuser angle, and motive nozzle throat, as shown in Table 3-1. All other parameters are indicated in

Table 3-2.

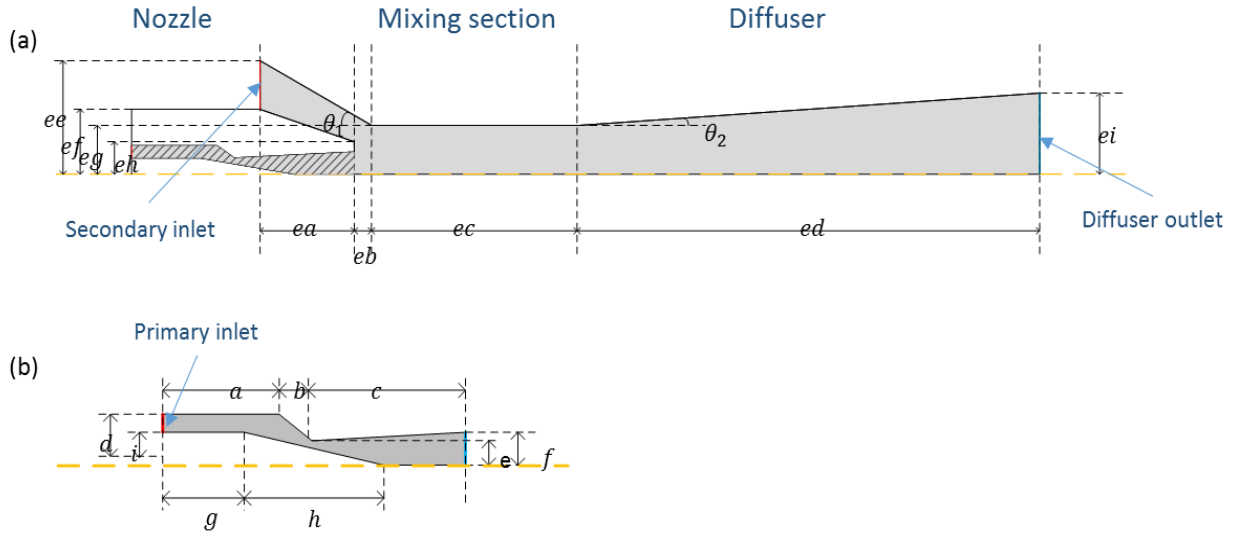


**Figure 3-1: Geometry of Designed Ejector (a) Ejector Inner Structure; (b) Motive Nozzle Structure**

The schematic of inner structure of the ejector is shown in Figure 3-1, the gray area indicates the flow region inside the ejector. The drawing of (b) shows the structure of motive nozzle, where the white region refers to the regulating needle to adjust throating area.

**Table 3-1: Optimized Non-Dimensional Values of the Designed Variables**

Variables	Non-dimensional Values
x1(dm), mixing chamber diameter	1
x2(Lm), mixing chamber length	8.36
x3(Ld), diffuser length	30.51
x4(alpha), motive nozzle diffuser angle [°]	0.96
x5(hd), motive nozzle throat diameter	0.15

**Table 3-2: Non-Dimension Values of the Other Ejector Geometries**

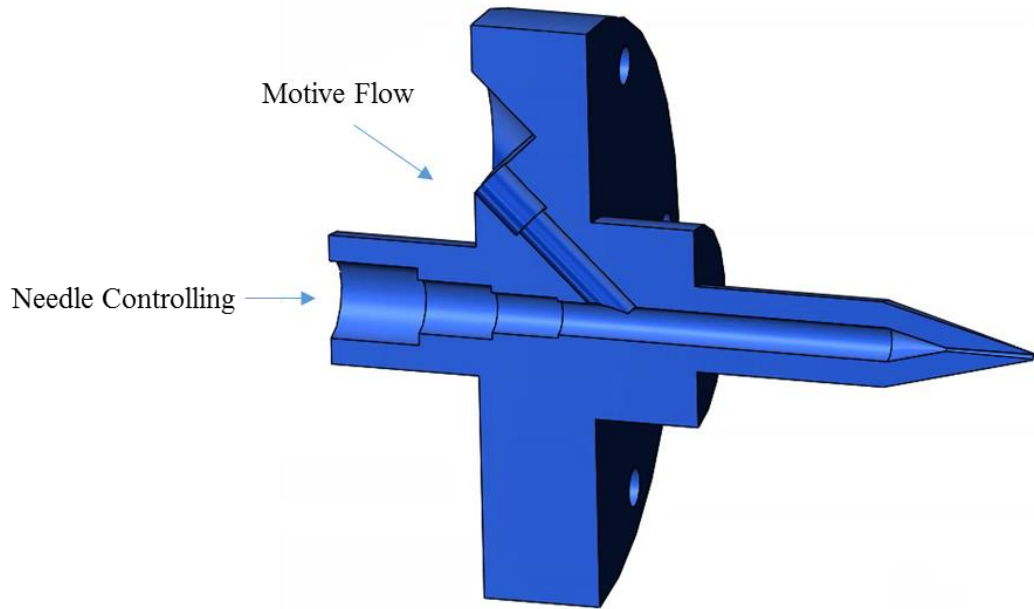
<b>Variables</b>	<b>Non-Dimensional Values</b>	<b>Variables</b>	<b>Non-Dimensional Values</b>
ea	6.81	a	6.08
eb	0.71	b	3.72
ee	4.87	c	5.30
ef	2.05	d	1.06
eh	0.22	f	0.15
ei	2.00	g	6.58
$\Theta_1$ [°]	30	h	4.77
$2*\Theta_2$ [°]	5		

Based on the ejector design provided, detailed computer aided design (CAD) drawings were developed for its manufacturing. A tolerance of 0.005 inch (0.127 mm) was implemented. Structures from Naduvath (1999) [33] were referenced for the part design.

### **3.1.1 Motive Nozzle Block**

The motive nozzle block is working as the motive nozzle in which the high pressure liquid refrigerant passes through and decreases the pressure at the outlet. Since a needle was designed to be inserted into the flow section, it was important to ensure that this thin needle was well aligned in the center. For a better alignment, a minimum needle length was desired. Since metal was used as the material due to the mechanical strength concern, the whole block should be compact to have less thermal mass. The reason for using stainless steel and brass was to prevent any potential mechanical damage and corrosion problem during experimental evaluation. To reduce as much pressure drop as possible in

the motive nozzle block, the flow region was designed to have a 45° angle with needle instead of 90°. The whole block was assembled using bolts.



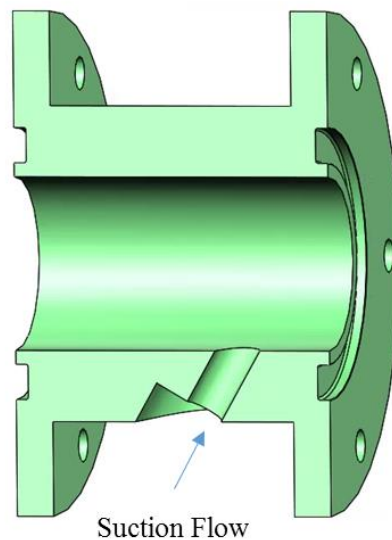
**Figure 3-2: 3D Drawing of Designed Motive Nozzle Block**

Figure 3-2 is the 3D drawing of the designed motive nozzle block. The 45° flow channel was for the motive flow, and a 1/16 NPT thread was used to connect 1/8 copper tube and the block. The straight channel was for the needle and one alignment piece was used to make sure the needle was well center-aligned. Details about the alignment piece are described in following section.

The whole part was simulated in SolidWorks for mechanical stress analysis, under pressure which was much higher than designed pressure. Simulation results show that this part has a reliable safety factor of around 11.

### 3.1.2 Suction Chamber Block

The suction chamber block was designed so that the suction flow could be sucked into the ejector. Then the suction flow is mixed with motive flow in the following mixing section. Theoretically, there is little mixing between two flows after the suction flow meets the motive flow. Motive flow keeps on expansion and forces the suction flow to reach in sonic velocity. In this process, the flow velocity becomes quite high so any mechanical gap would introduce disturbance to the ejector performance. That is the reason why mixing section is combined with diffuser section and pre-mixing divergent section. This suction chamber block only works as a support for other parts and a chamber for the suction flow.



**Figure 3-3: 3D Drawing of the Suction Chamber Block**

Figure 3-3 shows the drawing of suction chamber block with spacing for sealing O-rings. The spacing of O-ring was designed based on Parker Handbook [34]. To make sure the NPT fittings not interfere with the part, the suction flow channel was designed in a 70° angle from the cylinder center line.

Compared with other researches which used suction flow with a 90° turn, this design would have less pressure drop and the more uniform flow in the chamber.

### **3.1.3 Mixing and Diffuser Block**

As explained in previous section, the convergent part before the mixing section was combined with the mixing section and the diffuser section. Figure 3-4 shows the structure of mixing and diffuser section. At the outlet of the diffuser, 3/8 NPT thread was used. In addition to the flow section, pressure taps were designed to measure the pressures along the mixing section and in the diffuser. There were nine taps in total, where five of them in the mixing section. To make sure there was no conflict in assembling, the planes of the taps were tilted in some degree from the bolts plane, which is shown in assembly drawing.

According to the literature review, the mixing between the two flows are mainly happening in constant area mixing section and pressure has a large fluctuation along the flow direction. This is why multiple pressure taps were installed in constant area section. With the pressure taps, it was possible to find out the pressure profile inside the ejector, and to decide whether the ejector was at good mixing condition.

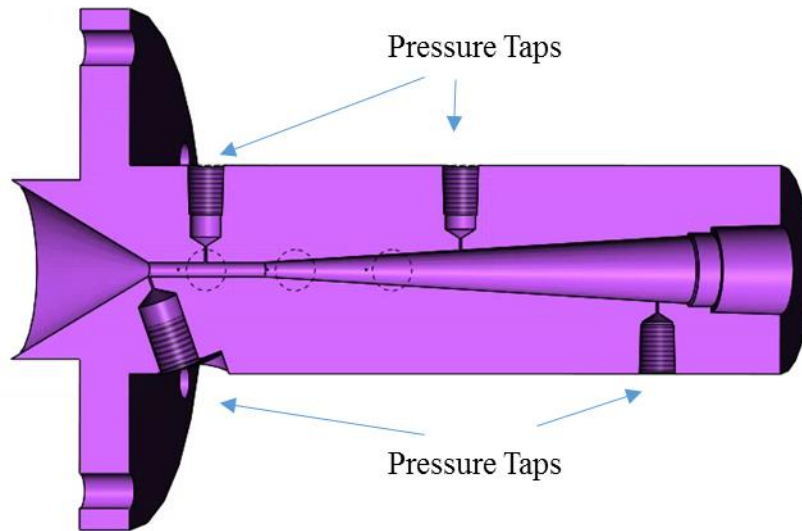


**Figure 3-4: 3D Drawing of the Mixing and Diffuser Block**

#### **3.1.4 Alignment Piece of the Needle**

As explained in motive nozzle blocks section, the needle position could still be off from the center due to large ratio of length to diameter although the design was optimized for shorter needle length. Therefore, an alignment piece was designed support the middle part of the needle. Figure 3-5 shows the drawing of the alignment piece. The needle was installed in the center space.

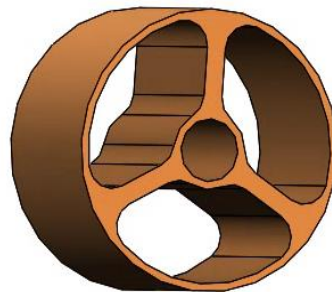


**Figure 3-5: 3D Drawing of Needle Alignment Piece**

The purpose of this part was to hold the needle in the center within the motive nozzle block with a minimum material. The length of this part was slightly longer than 1 cm, which was long enough to hold the needle.

### 3.1.5 Assembly of Ejector

The schematic of all parts assembly including the motive nozzle block, suction block, mixing and diffuser block, needle, alignment piece, and other fittings are shown in the Figure 3-6. On the left hand side, the needle was connected to a metering valve with a Vernier handle for precise control.

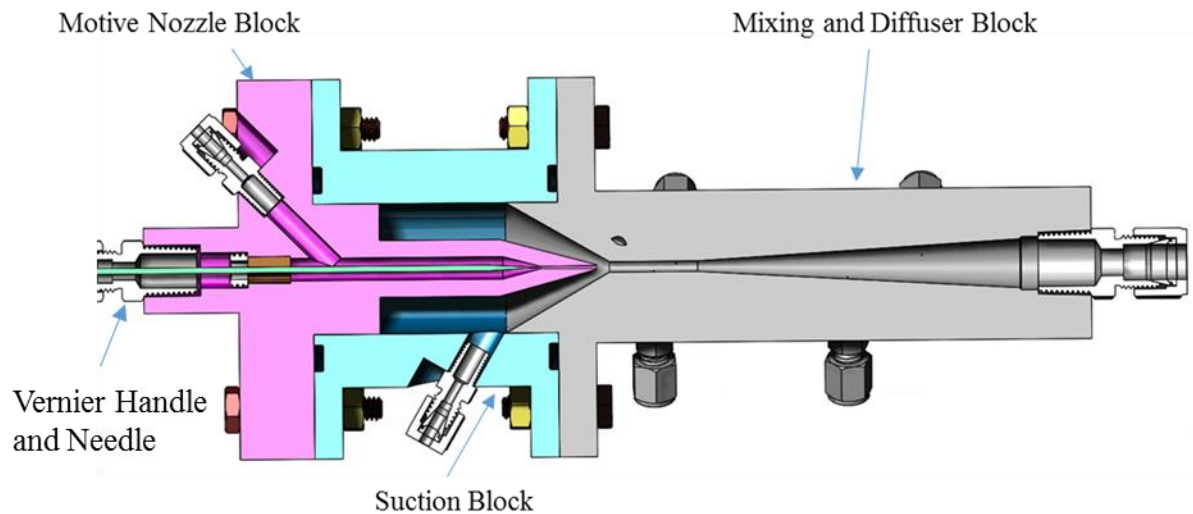
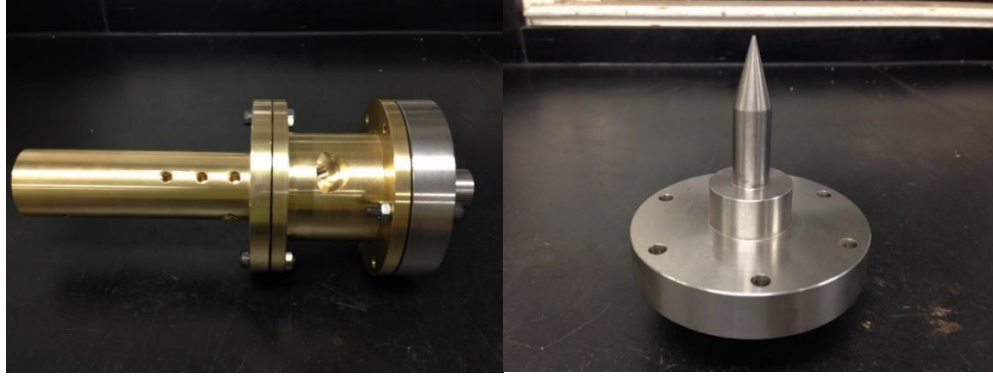


**Figure 3-6: Assembly Drawing of Designed Ejector**

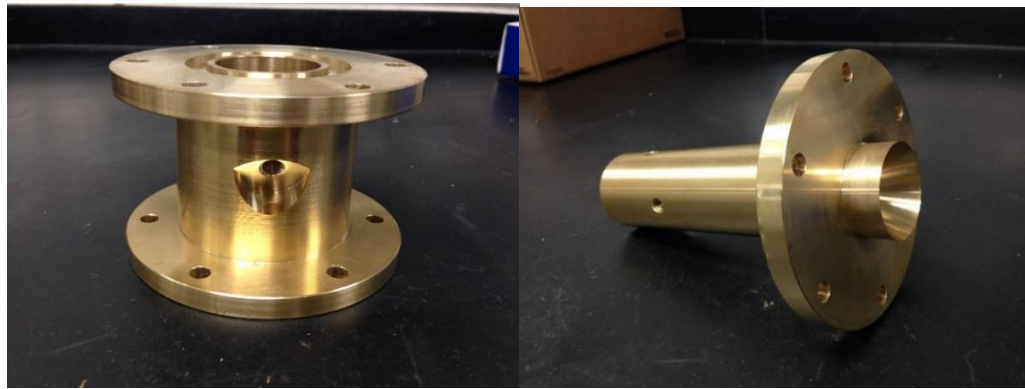
### 3.2 Ejector Fabrication

The ejector was manufactured using stainless steel and brass material as shown in Figure 3-7. Some main dimensions, such as nozzle throat diameter, and mixing section diameter, were checked for manufacturing accuracy. The manufactured ejector was in good agreement with design.



(a)

(b)



(c)

(d)

**Figure 3-7: Main Parts of Manufactured Ejector (a): assembly; (b): motive nozzle block; (c): suction chamber block; (d): mixing and diffuser block)**

Angle metering valve from Swagelok, SS-4MA2-MH, was chosen for needle connection.

Assembled needle was tightly attached the valve as shown in Figure 3-8.

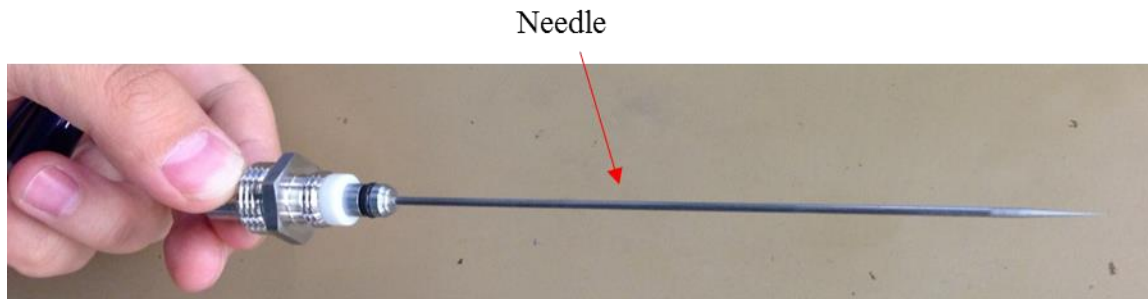
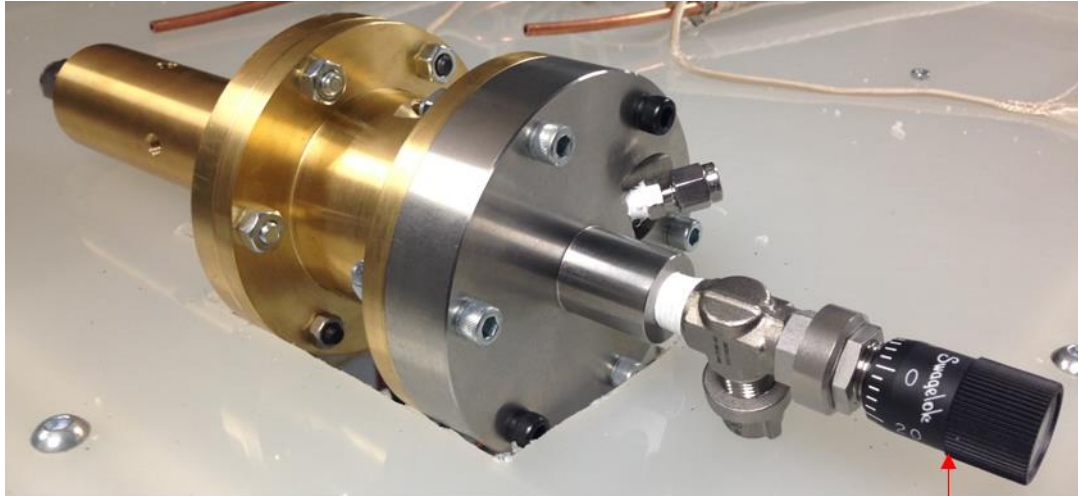


**Figure 3-8: Needle Connected to the Metering Valve**

The assembled needle control is shown in Figure 3-9. Another NPT port which is shown in the figure was closed with cap.



Vernier Handle

**Figure 3-9: Ejector Assembly with Needle Control**

### **3.3 Compressor**

Samsung variable speed compressor model (NC4EVA5ALM) shown in Figure 3-10 was chosen for the system. The control board transmitted 0-5 V square wave signal to the compressor to have different RPMs. The compressor RPM was controlled by the frequency of the signal. This compressor had a displacement volume of 15.31 cm<sup>3</sup>.



**Figure 3-10: Variable Speed Compressor for R600a System**

### **3.4 Condenser and Condenser Fan**

The designed ejector was needed to be tested under a wide range of conditions, so the selected condenser and its fan were chosen to meet the maximum possible capacity. Two parallel heat exchangers were bundled together and mounted on the frame board as shown in Figure 3-11. To ensure the good air flow to the condenser, the polypropylene housing was installed around the fan.

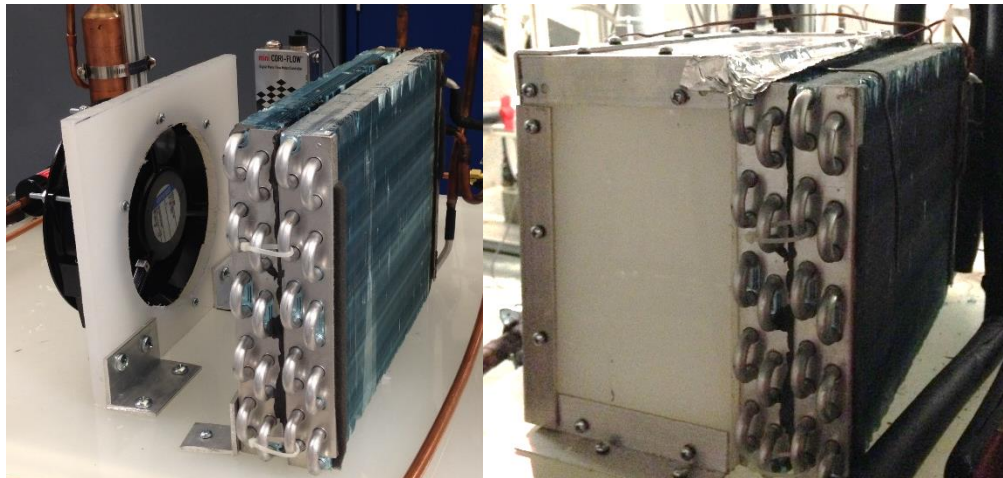


**Figure 3-11: Components and Housing of the Condensing Unit**

### 3.5 Electric Expansion Valve

The estimated flow rate of R-600a was below 1 g/s for the baseline cycle. Precise control of expansion device was desired to achieve target evaporating temperature. Sporlan SEI series electronic expansion valve (Figure 3-12) was selected for the system because it has very small step control, 1,596 steps. The valve was controlled by 4-20 mA signal. To prevent accidental close of the valve, one bypass metering valve was also installed.



**Figure 3-12: Electronic Expansion Device from Sporlan [35]**

### 3.6 Heaters

Electric heating tapes were used as a heat source for the evaporators, and controlled by VARIAC. The heating tapes were tightly wrapped around the copper tube and insulated with glass fiber. To prevent accidental heating of tube, which could cause explosion or leakage of R-600a, thermal switches, which could cut the heater off when temperature became higher than 40°C, were installed after each heater. Pictures of the evaporator heaters are shown in Figure 3-13.

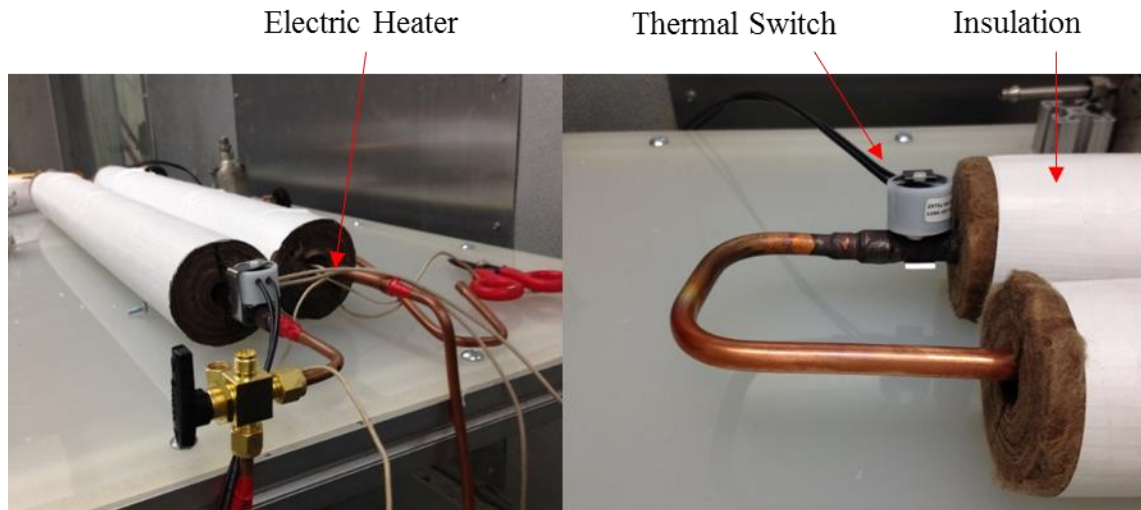


**Figure 3-13: Pictures of the Evaporator Heaters**

There were two more heaters applied in ejector cycle system with the same tube size and insulation setup.

### **3.7 Flash Tank**

Separation of the two-phase fluid after the ejector is important. One reason is to prevent liquid refrigerant flowing into the compressor and another reason is to ensure there is only liquid refrigerant flowing to the expansion valve. From Figure 3-14, it is seen that the flash tank used was a cylindrical tank which can separate liquid and vapor using centrifugal force. To observe the refrigerant level inside the flash tank, additional sight glass was installed close to the flash tank

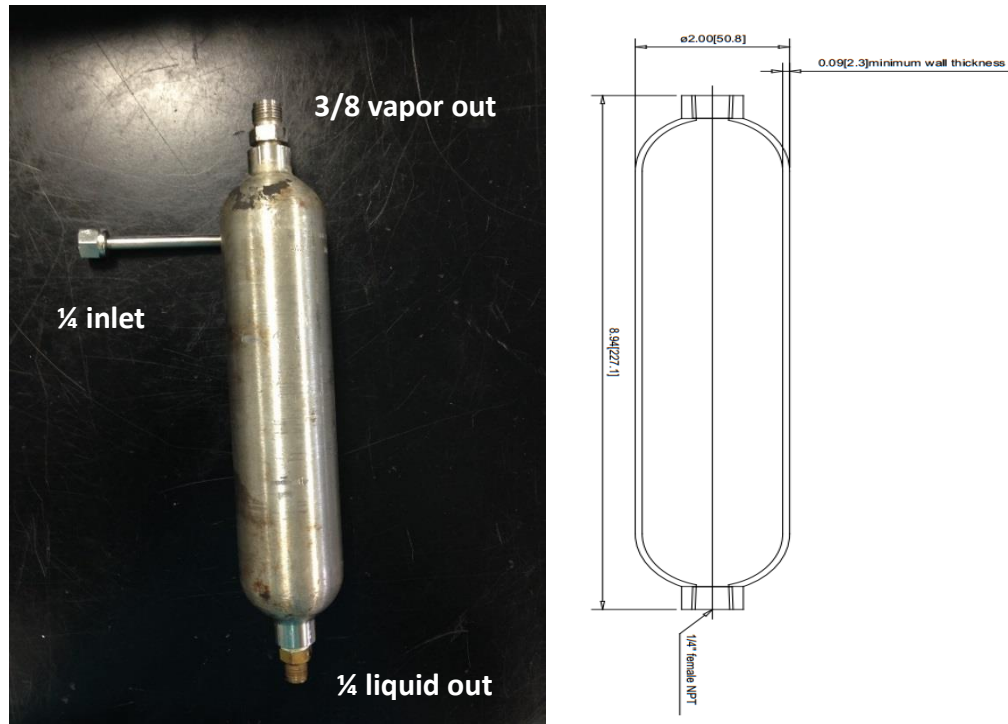


**Figure 3-14: Schematic of the Stainless Steel Flash Tank**

### 3.8 Test Facility Design

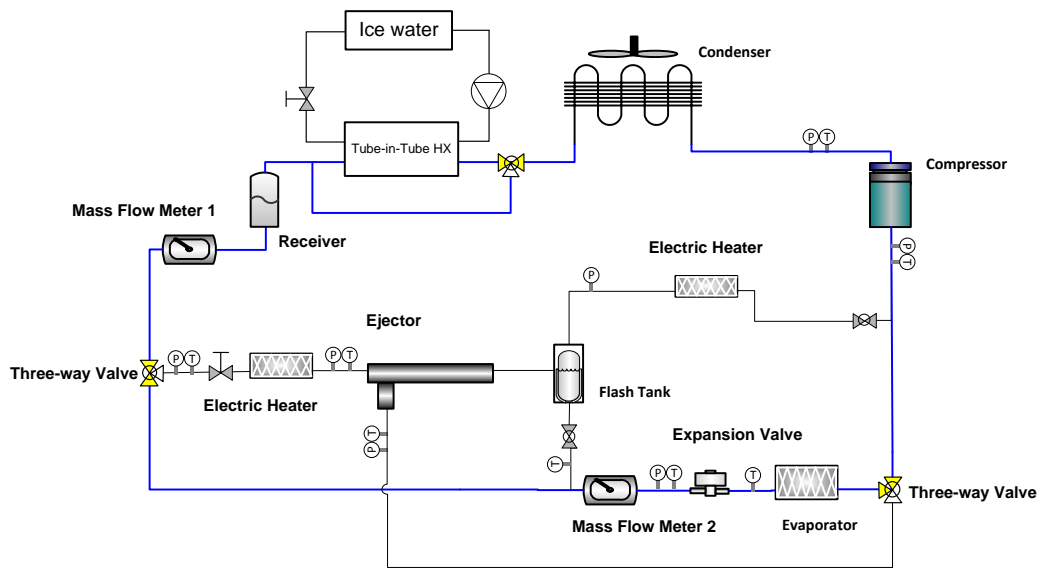
The goal of the experimental investigation was to evaluate the performance of the designed ejector, and to explore the potential of the ejector applied refrigeration system. So the system was designed to be evaluated under a wide range of operating conditions.

Figure 3-15 shows the initial design of the system which could switch the cycle configuration in two modes: (a) baseline VCC and (b) EERC. The blue line and red line indicate the flow in the cycle. The tube-in-tube HX was added to provide desired subcooling, which made it possible to have a good control on the motive flow pressure. Before the refrigerant entering to the ejector motive nozzle, a metering valve was installed to control the refrigerant pressure to the ejector and an electric heater was

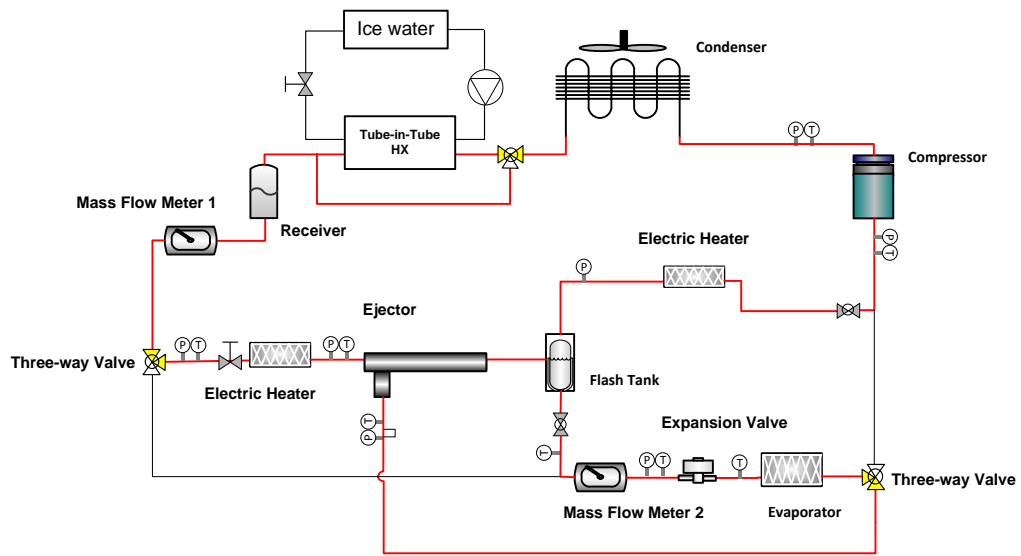
installed to control the refrigerant quality to a desired quality. Three-way valves were used to switch between the baseline VCC and the EERC.

After shakedown testing of the initial system design, a low entrainment ratio (0.08) was observed. Several possible factors which affected the system performance were as follows:

- Since there was no indicator of states after the flash tank, it was hard to diagnose the system operations;
- With 24 VDC power supply to the mass flow meter, there could be heat gain from the mass flow meter to the refrigerant-side. With this heat, the refrigerant flow to the expansion valve might become two-phase;
- Pressure drop along the suction line and gravity effect caused a low entrainment flow rate;
- After the system was shut down, oil might be trapped in the suction line, which could cause problem for the next start up.



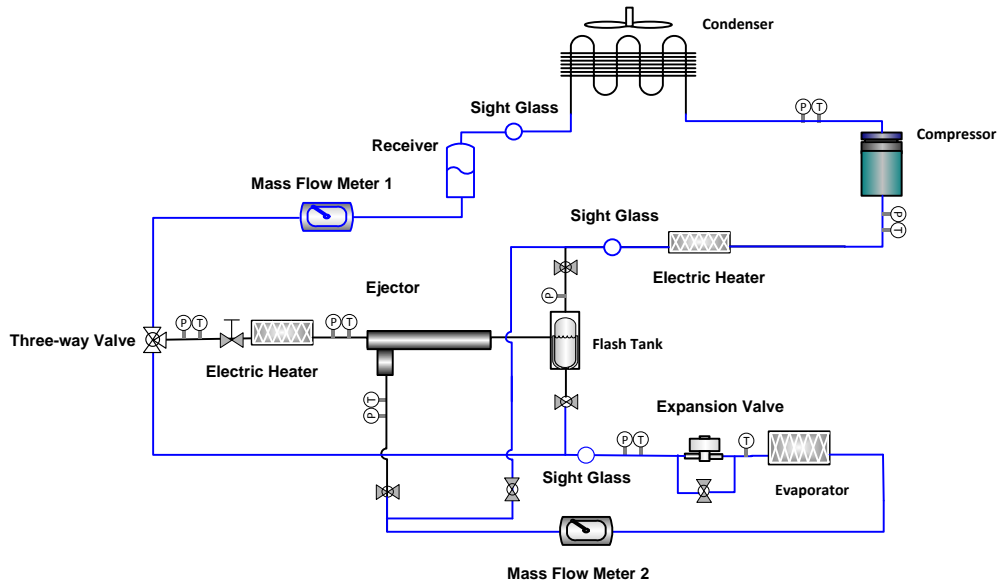
(a)



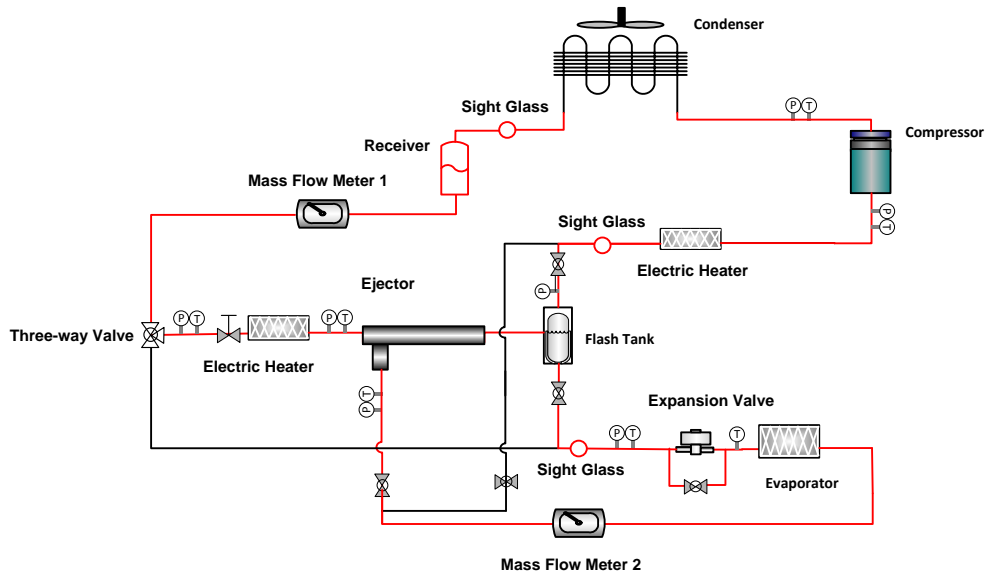
(b)

**Figure 3-15: Schematic of the Initial System Configurations with Two Operational Modes: (a) Baseline (b) EERC**

Based on lessons learned from the preliminary shakedown tests, the test facility was modified as shown in Figure 3-16.



(a)



(b)

**Figure 3-16: Modified Schematic of Ejector System in (a) Baseline VCC and (b) EERC**

Two sight glasses were installed after the flash tank to monitor the refrigerant phase state, the mass flow meter was relocated after the evaporator to reduce heating effect, the

suction line length was shortened to minimize the pressure drop, and the suction line was reconstructed at the same height to prevent gravity effect. For the oil trap problem, the piping connection was redesigned and once cycle configuration was turned to baseline VCC mode, the whole suction line was flushed with high velocity refrigerant.

For heaters, there were three of them: the one before the motive nozzle of the ejector was expected to have 0 to 400 W capacity to change the quality for 1 g/s flow rate; the one before the compressor was expected to provide heat for refrigerant to reach superheated state, the heat absorbed here could also be used for a higher temperature evaporator; and the evaporator heater was expected to provide heat source for a lower temperature evaporator with a 100 to 200 W capacity based on different flow rates.

Sight glasses can be helpful to diagnose the refrigerant's state. When two-phase refrigerant appeared in the flash tank sight glass of the vapor line, the power of the electric heater before the compressor needed to be increased to evaporate liquid refrigerant before the compressor. When two-phase refrigerant appeared in the liquid sight glass, there might not be enough liquid refrigerant in flash tank supplied to the evaporator and the opening of the EEV should be changed according to the situation. In addition to the two new ones added to the system, there was another one installed after the receiver as an indicator of subcooling state.

R-600a, also known as isobutane, is one of the natural refrigerants and was used as the working fluid in this study. GWP of R-600a is only 3 so that it is one of the desired refrigerants in refrigeration. However, its flammability becomes the biggest issue for applying it in large charge range. Several safety protections were installed for unexpected emergency.

In the system, the controllers of heaters, compressor, fan and EEV, the power consumption instruments, and safety switches were all needed to be connected electrically. For power supply, there were two types of powers provided to the system: 208VAC for compressor and 115VAC for heaters. Figure 3-17 provides the schematic of electronic component connection. Compressor, fan, and heater switches were a manual type. In each power line, a solid state relay was installed. For easy control of the heater, VARIACs were installed to manually adjust the line voltage supplied to the heaters. Thermal protection switches were installed so that if the heater temperature exceeded 40°C, the power could be cut off.

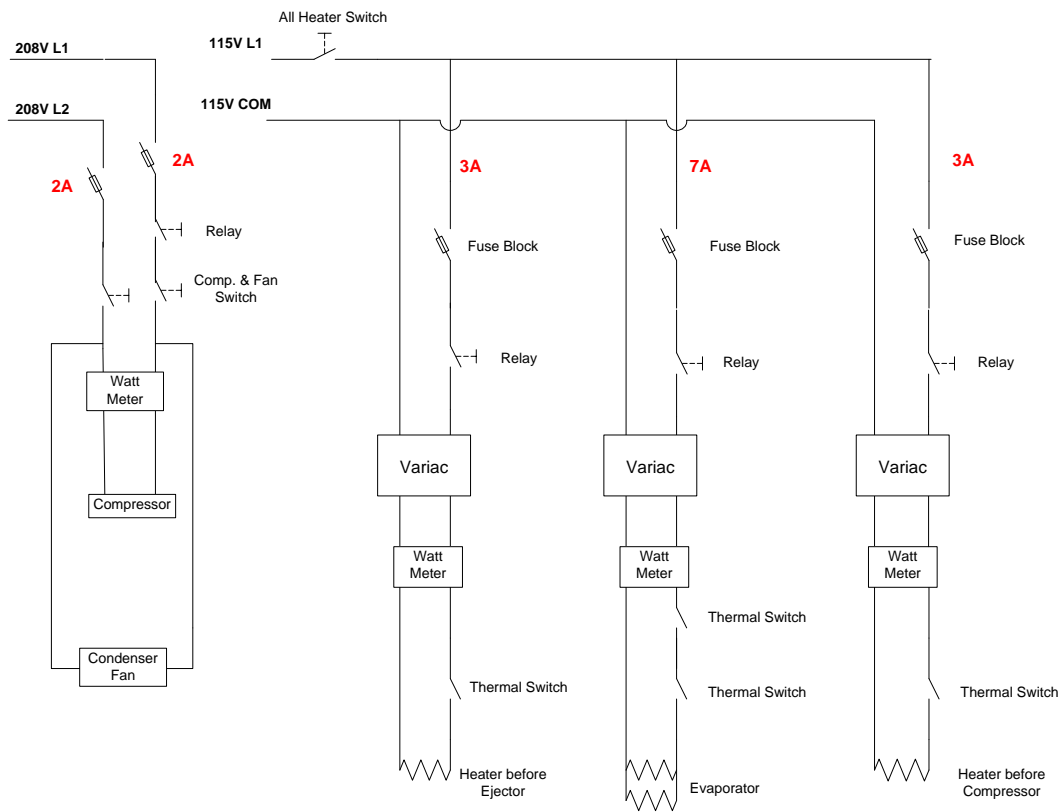


**Figure 3-17: Electrical Schematic**

The red color numbers indicate the maximum current through each line. The size of the fuse was decided by this number. The fan used in the condensing unit was a 12 VDC axial fan without speed control so that the power was supplied accordingly with DC power supply. As for electronic expansion valve, 24 VDC power was needed to drive the step motor inside. An analog output signal of 4-20 mA was used to control between 0-100% openings of valve.

### **3.8 Test Facility Construction**

The whole test facility was constructed based on test schematics. Figure 3-18 to Figure 3-21 show the pictures of the test facility. The test facility was constructed on a 4 feet x 2 feet x 4 feet frame built with 80-20 bars and polypropylene. The electric box was installed on the side of the frame, and DAQ system was installed in the front-side.

On the lower level of the test facility, compressor, condensing unit, mass flow meter, and receiver were mounted as shown in Figure 3-19. Most of the copper tubes were connected by brazing to prevent possible leakage. On upper level of the test facility, ejector, flash tank, evaporator, and expansion valve were mounted. Two heaters were installed under the frame. Flash tank was mounted vertically.

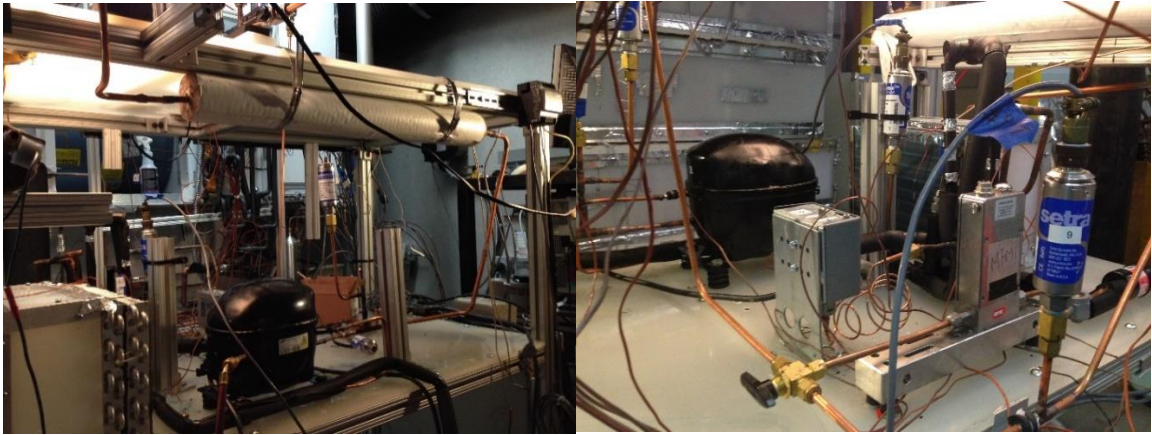


**Figure 3-18: Overview of Bottom Level Test Facility**

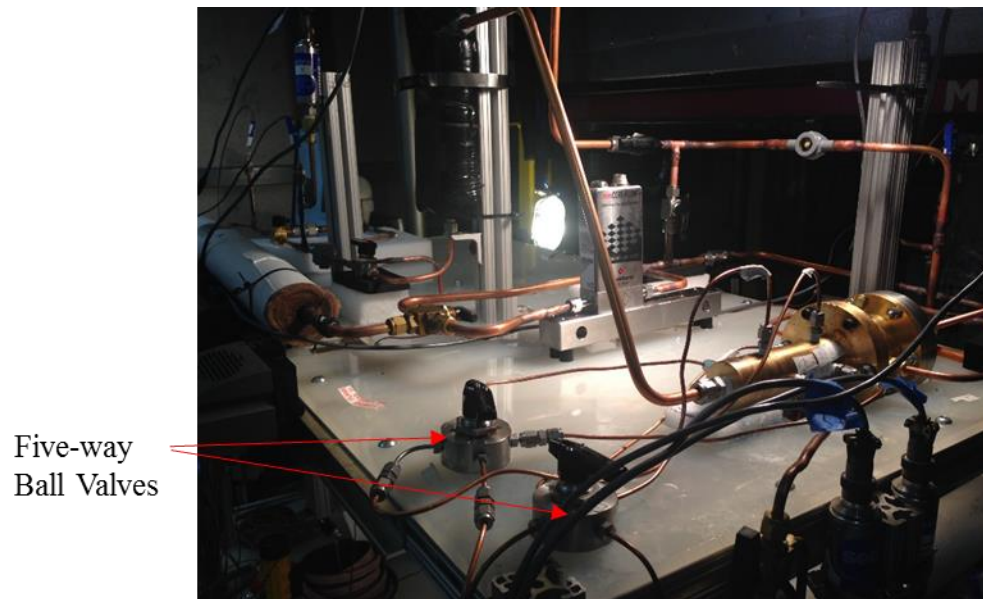


**Figure 3-19: Upper Level Test Facility**

In Figure 3-19, besides all components mentioned before, there were two five-way ball valves working as pressure manifold. By switching among pressure taps, certain pressure tap was connected to pressure transducers.

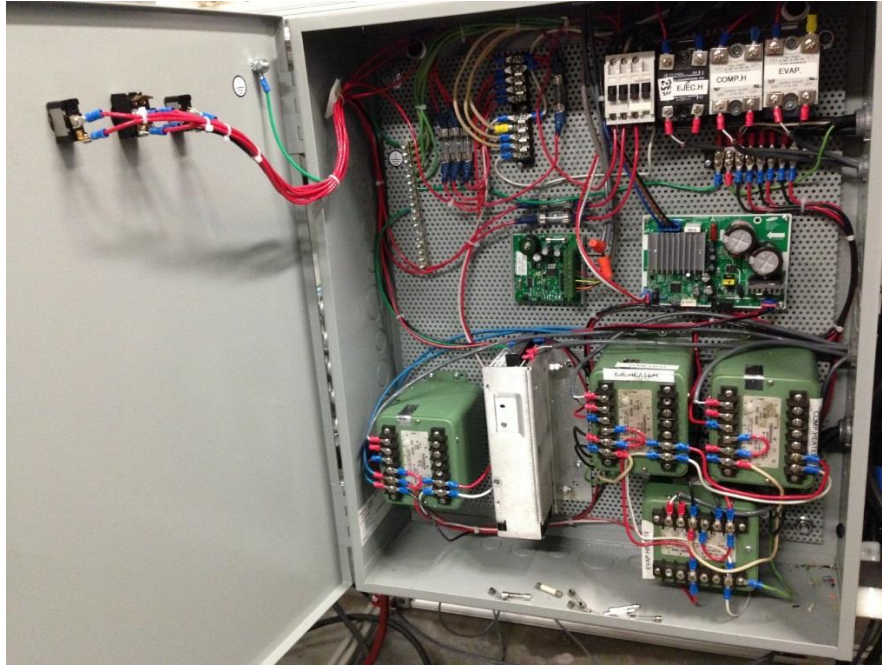


**Figure 3-20: Electric Box Overview**

Figure 3-20 is the overview of electric box inside. Three manual switches were mounted on the door. The box was well grounded. The 115 VAC was supplied to variacs on the lower level of test facility connected to watt meter and then to the heaters.

Figure 3-21 shows the Data Acquisition (DAQ) system, FieldPoint modules. Two Analog Input (AI) modules were used for inputting pressures, mass flow rate and power consumptions; one Analog Output (AO) module for controlling EEV; one Digital Output (DO) module for controlling heater relays; and two Thermocouple (TC) modules for temperatures.



**Figure 3-21: Data Acquisition System Setup**

### **3.9 Instrumentation**

Pressures and temperatures were needed to determine the state points of the system. And mass flow meters were used for the flow rate, entrainment ratio and capacity calculation of the system.

#### **3.9.1 Thermocouples and Pressure Transducers**

The temperature range in the system was between  $-30^{\circ}\text{C}$  to  $80^{\circ}\text{C}$  so that typical T-type thermocouple were used with 0.5 K accuracy as shown as Figure 3-22. There were eight in-stream thermocouples used for measuring the refrigerant temperature at each state point. More surface thermocouples were also used in multiple locations to measure temperatures of interest. Since surface thermocouples were directly attached on the copper tube instead of exposed to refrigerant stream, there was an error depending on the conditions. However, with a good thermal conductivity of copper, this error was not significant.

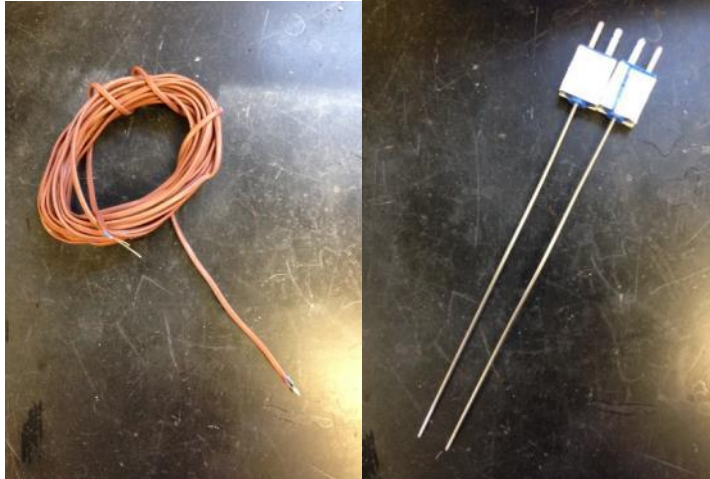


**Figure 3-22: Surface (left) and In-stream (right) T-type Thermocouples**

Same with thermocouples, pressure transducers (Figure 3-23) were installed to measure the pressure at each state point. To have a better accuracy of pressure measurement, the most appropriate range, 0-689 kPa absolute pressure, was applied, with a 0.05% full scale uncertainty. All pressure transducers were calibrated to maintain high accuracy.



**Figure 3-23: Setra AccuSense High Accuracy Pressure Transducers.**

In addition to the pressure transducers needed for state point calculation, two more were used for pressure profile measurement inside ejector. As shown in chapter 3.1.3, there

were nine pressure taps in mixing and diffuser sections. Since this study was intended for steady state testing, it was not needed to know all pressures at each tap at the same time. Thus to decrease the cost for pressure transducers, nine pressure taps were divided into two groups: one includes five taps in mixing section and another includes four taps in diffuser section. Pressure taps were connected to five-way ball valves, each pressure could be known by switching the ball valve to the certain position.

### 3.9.2 Mass flow meters

Due to the small flow rate of the system, Bronkhorst Coriolis mass flow was chosen at a range of 0 - 1 g/s flow rate for R-600a. The flow meters were calibrated before testing to ensure that the flow rate reading was reliable.



**Figure 3-24: Bronkhorst Mini CORI-FLOW Meters**

Since Coriolis flow meter has a higher accuracy for liquid phase than gas phase, the motive flow's mass flow meter was installed at the liquid line. However, the suction flow's mass flow meter brought in the heat that could affect the refrigerant state.

Therefore, it was relocated to the vapor line. In the baseline mode, two mass flow meters

were installed in series so that they would measure the same flow rate. While in EERC mode, one was measuring the motive refrigerant flow and another was measuring the suction refrigerant flow rate.

All other related instrumentation are listed in Table 3-3, showing the manufacturer, model number, range and systematic uncertainty specifications. All instruments were accurately set to a reasonable range based on test conditions.

**Table 3-3: Specifications of Instruments**

<b>Instrument</b>	<b>Type</b>	<b>Brand</b>	<b>Model</b>	<b>Range</b>	<b>Systematic uncertainty</b>
Mass flow meter	Coriolis	Bronkhorst	M14-AAD-22-O-S	0-1g/s	$\pm(0.2\% \text{ Rd} + 0.002 \text{ g/s})$
Pressure	Strain	Setra	Accusense	0-100psia	$\pm 0.05\% \text{ F.S}$
In-stream thermocouples	T-type	Omega	TMQSS062 G6	(-250)-350°C	$\pm 0.5^\circ\text{C}$
Watt Meter	Watt transducer	Ohio Semitronics	PC5-002X5	0-1000W	$\pm 0.5\% \text{ F.S}$
Watt meter	Watt transducer	Ohio Semitronics	GW5-020D	0-4000W	$\pm 0.2\% \text{ F.S}$

### 3.10 Test Conditions

For the baseline test, the designed working conditions were in typical conditions of a refrigerator with an evaporating temperature at  $-10^\circ\text{C}$  and a room temperature at  $25^\circ\text{C}$ .

The temperature indicated that low side pressure was around 100 kPa absolute, with a little bit variation depending on the pressure drop through refrigeration line. The temperature of superheated vapor entering the compressor suction was assumed to be the same as room temperature. Then, the degree of superheat would be 35 K, which is typical value in the refrigerator.

For the EERC test, it was desired to reach similar conditions to the baseline for comparison of performance. In addition to the temperature and pressure conditions, the ejector was designed to have a 0.4-0.6 entrainment ratio. Additional tests were also necessary to explore the potential of ejector cycle under various operating conditions, and the throat opening of ejector nozzle was controlled by the needle.

### 3.11 Data Reduction

#### 3.11.1 Baseline

It was necessary to compute the system COP and the evaporator capacity to ensure that all measured data were in a reasonable range of a typical refrigerator application. To validate the reliability of experiment result, the energy balance needed to be checked for components and the system. System's energy should be balanced according to the following equation (1).

$$W_{compressor} + Q_{heater} + Q_{gain} = \dot{m}\Delta h_{condenser} + Q_{loss} \quad (1)$$

In addition to the whole system, evaporator's energy should be balanced between heater side and refrigeration side as follows:

$$Q_{evaporator} + Q_{loss} = \dot{m}\Delta h_{evaporator} \quad (2)$$

Since the system is used for refrigerator application, the system COP is defined as:

$$COP_C = \frac{Q_{evaporator}}{W_{compressor}} \quad (3)$$

Although there could be heat gain before the evaporator after the expansion device in the test facility, this part of energy was not included in the COP calculation.

### 3.11.2 EERC

The COP defined in the EERC system is different from the baseline. In EERC, the refrigerant section after flash tank before the compressor also had a cooling effect. Therefore, this cooling capacity was also included in the COP definition as shown in Eq. (4).

$$COP_C = \frac{Q_{evaporator} + Q_{high\ temp\ evaporator}}{W_{compressor}} \quad (4)$$

For EERC, one important parameter determining the system performance is an entrainment ratio ( $w$ ), which is the ratio of the suction flow rate and motive flow rate as shown in Eq. (5). The higher the entrainment ratio is, the better COP the system has.

$$w = \frac{\dot{m}_{suction\ flow}}{\dot{m}_{motive\ flow}} \quad (5)$$

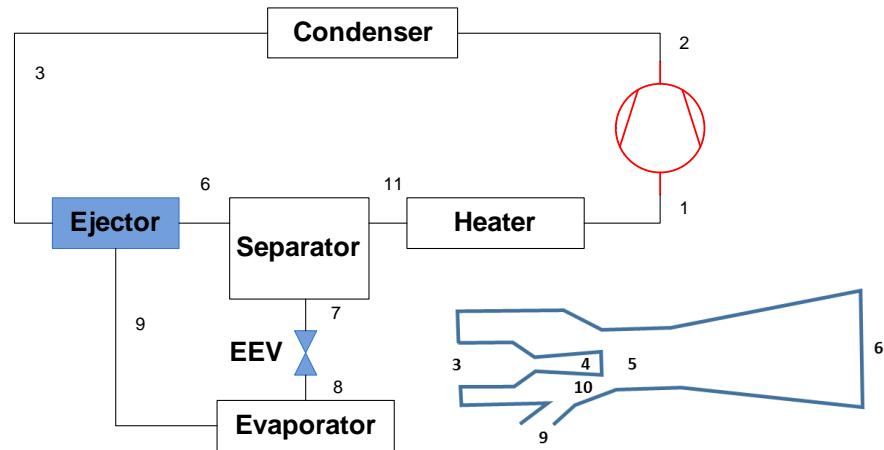
In addition to system level analysis, it's worthwhile to analyze the ejector performance alone. The reason for an EERC system to have a higher COP is that the ejector have a pressure lift from the suction pressure level. Since the refrigerant from the evaporator can be compressed to an intermediate pressure level, the compressor work is reduced. With the inlet conditions of ejector and designed efficiency, pressure lift can be estimated using energy and momentum conservation equations. To make it easier to understand equations, all state points in the equations are referred to Figure 3-25.

The first process inside ejector is the expansion of the motive flow, which is the process from state 3 to state 4:

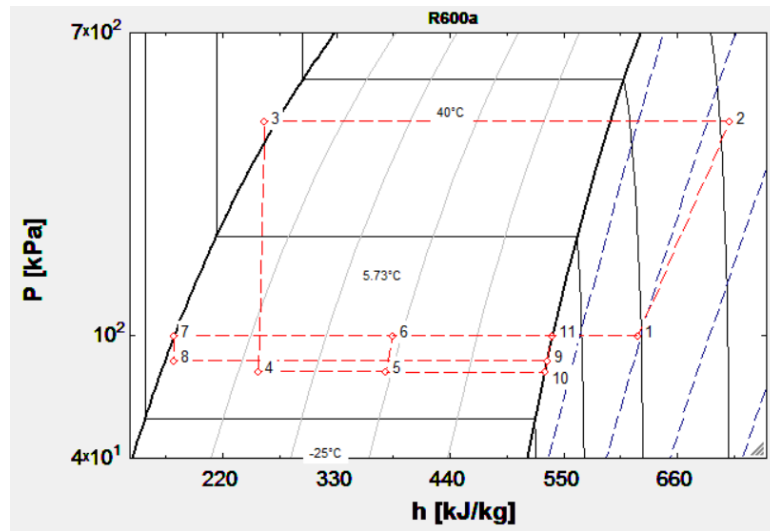
$$h_{4s} = f(P_4, s_3) \quad (6)$$

$$\eta_{mn} = \frac{h_3 - h_4}{h_3 - h_{4s}} \quad (7)$$

$$h_3 + \frac{u_3^2}{2} = h_4 + \frac{u_4^2}{2} \quad (8)$$



(a) EERC schematic



(b) P-h diagram

**Figure 3-25: Simplified Schematic and P-h Diagram of EERC**

The second process is the suction of suction flow from state 9 to state 10 as shown in Eqs. (9) - (11). Since the pressure differences among states 4, 5, and 10 are very small, it was reasonably assumed that pressures at this three states were the same. Using the

pressure assumption at state 4 and the entropy at state 9, isentropic enthalpy at state 10 can be calculated (Eq. (9)). Then with the designed suction nozzle efficiency, enthalpy at state 10 can be obtained from Eq. (10). Eq. (11) is used to calculate the velocity at state 10.

$$h_{10s} = f(P_{10}, s_9) \quad (9)$$

$$\eta_{sn} = \frac{h_9 - h_{10}}{h_9 - h_{10s}} \quad (10)$$

$$h_9 + \frac{u_9^2}{2} = h_{10} + \frac{u_{10}^2}{2} \quad (11)$$

The third process is the mixing of two flows (state 4 to 5 and 10 to 5) as shown in Eqs. (12) - (13). During mixing, the pressure may fluctuate around pressure at state 5 but it's still reasonable to use a constant pressure mixing model. Eq. (12) shows the momentum equation for calculating the velocity at state 5. And Eq. (13), energy equation, uses the velocity at state 5 to calculate enthalpy at state 5.

$$P_{10}A_{10} + P_4A_4 + \eta_m(\dot{m}_{mf}u_4 + \dot{m}_{sf}u_{10}) = P_5(A_4 + A_{10}) + (\dot{m}_{mf} + \dot{m}_{sf})u_5 \quad (12)$$

$$\dot{m}_{mf}\left(h_4 + \frac{1}{2}u_4^2\right) + \dot{m}_{sf}\left(h_{10} + \frac{1}{2}u_{10}^2\right) = (\dot{m}_{mf} + \dot{m}_{sf})\left(h_5 + \frac{1}{2}u_5^2\right) \quad (13)$$

The forth and the last processes are the pressure recovery from state 5 to 6 as shown in Eqs. (14) - (16).

$$h_5 + \frac{u_5^2}{2} = h_6 + \frac{u_6^2}{2} \quad (14)$$

$$\eta_d = \frac{h_{6s} - h_5}{h_6 - h_5} \quad (15)$$

$$P_6 = f(h_{6s}, s_5) \quad (16)$$

The estimated pressure was compared with test result later to see whether the ejector was working under designed condition.

### 3.12 Uncertainty Analysis

All systematic uncertainties can be obtained from manufactures. Random errors are obtained from standard deviation (Eq. 18), which is obtained from real-time data recorded from LabVIEW (Laboratory Virtual Instrument Engineering Workbench) DAQ software.

$$\varepsilon_{total} = \varepsilon_{sys} + \varepsilon_{STD} \quad (17)$$

Where:

$\varepsilon_{total}$  = total uncertainty of a measured value

$\varepsilon_{sys}$  = systematic uncertainty of a measured value

$\varepsilon_{STD}$  = random uncertainty of a measured value

$$\varepsilon_{STD} = \sqrt{\frac{1}{N-1} \sum_{j=1}^N (x_j - \bar{x})^2} \quad (18)$$

Where:

$N$  = number of data points in the collected data set

$j$  = data point index

$x_j$  = measured variable data point at index  $j$

$\bar{x}$  = average of the measured variable over the entire data set

#### **4. Test Results and Data Analysis**

Both tests of the baseline VCC and EERC were conducted for performance measurement. Since the current research was focused on the steady state performance, all test results were recorded for at least one hour after the cycle reached its steady state condition and the last half hour results were used for data analysis. Detailed results and data analysis were reported in the following sections.

##### **4.1 Baseline VCC Tests Results**

Since a liquid receiver was installed in the system in order to reduce the charge sensitivity, no charge optimization was needed. Total 500 g of R-600a was charged into the system to ensure that there was enough refrigerant even after the charge migration during transient operation period. The compressor frequency was set at 55 Hz. By controlling the opening of electronic expansion valve (EEV), medium and low evaporating temperature test conditions ( $-10^{\circ}\text{C}$  and  $-28^{\circ}\text{C}$ ) were reached. It took about one hour before the system reached its steady state condition, and test data was recorded for next half hour and averaged over time.

The time averaged values of  $-10^{\circ}\text{C}$  evaporating temperature are shown in Table 4-1. In summary, the compressor was working at a pressure ratio of 5.06 with a power consumption of 91.1 W. Heater provided 284.45 W heat to the evaporator. There was a 3.1 % energy unbalancedness for evaporator.

**Table 4-1: Summary of Baseline Test Results at (-10°C) Evaporating Temperature**

<b>Variables</b>	<b>Unit</b>	<b>Baseline Result</b>	<b>Systematic Uncertainty</b>	<b>Random Uncertainty</b>	<b>Total Uncertainty</b>
Compressor Discharge Pressure	kPa	499.3	0.34	2.56	2.90
Condenser Outlet Pressure	kPa	488.5	0.34	0.49	0.83
Evaporator Inlet Pressure	kPa	107.4	0.34	0.32	0.66
Compressor Suction Pressure	kPa	98.6	0.34	0.27	0.61
Compressor Discharge Temperature	°C	53.9	0.5	0.09	0.59
Condenser Outlet Temperature	°C	25.1	0.5	0.06	0.56
Evaporating Temperature	°C	-10.2	0.5	0.08	0.58
Compressor Suction Temperature	°C	22.7	0.5	0.08	0.58
Room Temperature	°C	24.7	0.5	0.10	0.60
Mass Flow Rate	g/s	0.88	0.003	0.004	0.007
Compressor Power Consumption	W	91.1	0.27	0.36	0.63
Evaporator Heater Capacity	W	284.45	0.21	1.09	1.30
Refrigeration-side Evaporator Capacity	W	293.51	1.65	1.35	3.00
Cooling COP	-	3.1	0.02	0.02	0.04

In addition to -10°C condition, a lower evaporating temperature condition test was also conducted at -28°C as a benchmarking for EERC, as shown in Table 4-2. In this condition, the compressor was working at a pressure ratio of 8.7 with a power consumption of 54.4 W. Heater provided 103.86 W heat to the evaporator. There was a 17.7% energy unbalancedness for evaporator. One thing to be noted is that the system COP was 1.9, which is quite high at this low evaporating temperature. One of the reasons is that R-600a has a larger latent heat and a less pressure ratio than those of R-134a at the

same operating condition. As compared with the -10°C test, the high side pressure shows lower value. The reason was that in this condition the compressor suction pressure was only 45.6 kPa, which resulted in a lower discharge pressure.

**Table 4-2: Summary of Baseline Test Results at (-28°C) Evaporating Temperature**

Variables	Unit	Baseline	Systematic	Random	Total
		Result	Uncertainty	Uncertainty	Uncertainty
Compressor Discharge Pressure	kPa	397.2	0.34	2.15	2.49
Condenser Outlet Pressure	kPa	392.6	0.34	1.75	2.09
Evaporator Inlet Pressure	kPa	51.3	0.34	0.58	0.92
Compressor Suction Pressure	kPa	45.6	0.34	0.83	1.17
Compressor Discharge Temperature	°C	50.7	0.5	0.38	0.88
Condenser Outlet Temperature	°C	25.7	0.5	0.04	0.54
Evaporating Temperature	°C	-27.9	0.5	0.25	0.75
Compressor Suction Temperature	°C	25.7	0.5	0.14	0.64
Room Temperature	°C	25.3	0.5	0.14	0.64
Mass Flow Rate	g/s	0.37	0.003	0.001	0.004
Compressor Power Consumption	W	54.4	0.27	0.42	0.69
Evaporator Heater Capacity	W	103.86	0.21	2.68	2.89
Refrigeration-side Evaporator Capacity	W	126.2	1.16	0.35	1.51
Cooling COP	-	1.9	0.01	0.05	0.06

## 4.2 Energy Balance Analysis

As stated before, there is a 17.7 % deviation in energy balance of the evaporator. After checking the uncertainty of instrument and comparing with  $-10^{\circ}\text{C}$  test result, the only reason that causes this large energy unbalance should be the heat gain from the environment. In the test facility, there was about two meters long tubes before the evaporator and around the expansion device (including exposed area of expansion device). Although the tube was well insulated, there was still a small heat flux through the insulation. Considering the total capacity of evaporator was 100 to 300 W range, any heat gain around 10 W could make a difference in its energy balance. In order to investigate this heat gain, two more tests were conducted under different temperature difference between the evaporating and ambient temperatures.

The test conditions were: (1) evaporating temperature at  $-28^{\circ}\text{C}$  with a room temperature of  $25^{\circ}\text{C}$ ; (2) evaporating temperature at  $-18^{\circ}\text{C}$  with a room temperature of  $25^{\circ}\text{C}$ ; (3) evaporating temperature at  $-28^{\circ}\text{C}$  with a room temperature of  $32.2^{\circ}\text{C}$ . The corresponding temperature differences were: (1) 53 K; (2) 43 K; and (3) 60.2 K, respectively. The evaporator capacity was calculated in each case and compared to the heater power supplied.

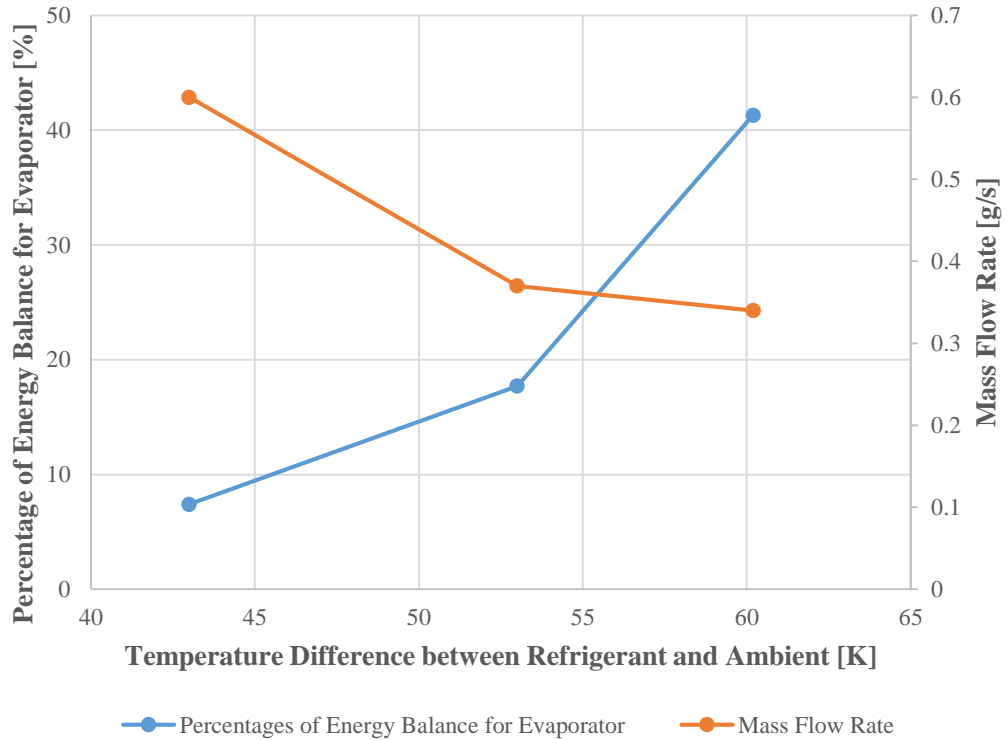


**Figure 4-1: Percentage of Energy Balance Deviation for Evaporator under Various Conditions**

Figure 4-1 provides the trend of energy balance in evaporator under different temperature differences. From the plot, it can be observed that the energy balance increases more with temperature difference. This increase could be due to two following reasons. One is because the large temperature difference causes a larger heat flux through the same tube and insulation. Another reason is that the same amount of heat gain has a larger effect to the smaller evaporator capacity. With the baseline test results and facility dimensions, it was possible to estimate the heat gain from the environment. The section for heat gain was assumed to be in a tubular shape regardless of their actual complex shapes for expansion device and in-stream thermocouples.

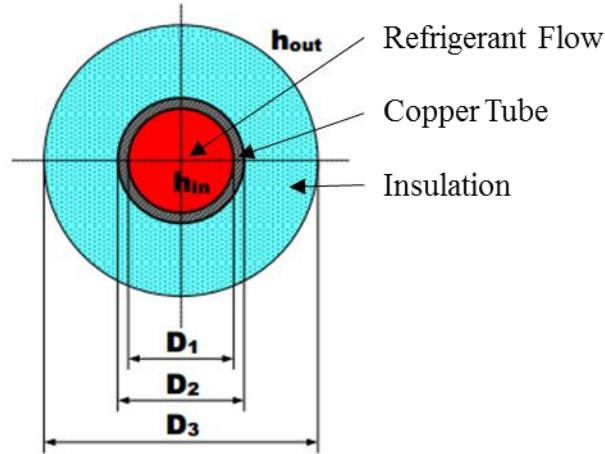


**Figure 4-2: Dimensions of Insulated Tubes**

Dimensions of insulated tubes are shown in Figure 4-2. Red, gray, and blue colored sections indicate the refrigerant flow section, tube thickness, and insulation, respectively.

With the flow rate and tube dimensions, Reynolds number was evaluated by using Eq.

(19). The fluid properties were calculated at the evaporator inlet state.

$$Re = \frac{\rho u D}{\mu} = \frac{\rho \frac{\dot{m}}{\rho A_p} D}{\mu} = \frac{\dot{m} D}{A_p \mu} = 641.6 \quad (19)$$

The laminar-to-turbulent transition Reynolds number inside a circular tube is around 2,300. Therefore, the refrigerant flow in this case was definitely laminar flow. The analysis of Nusselt number in laminar flow condition is well established under uniform surface temperature condition for circular tubes. The Nusselt number in test condition was 3.66. With the heat transfer coefficients, overall heat transfer coefficient ( $U_{overall}$ ) between the refrigeration and ambient air was calculated as:

$$U_{overall} = \frac{1}{\frac{D_3}{D_1 U_{ref}} + \frac{D_3 \ln\left(\frac{D_3}{D_2}\right)}{2k_{insulation}} + \frac{1}{U_{air}}} \quad (20)$$

In the equation above, the term considering the copper conduction was neglected later because copper has a very high thermal conductivity as compared with the insulation material.

The whole test facility was installed inside an environmental chamber whether the forced convection was used for air temperature control. Therefore, the air at the surface of the insulation was not absolutely still and the heat transfer coefficient on the air side was assumed between the typical natural convection and typical forced convection condition. In the estimation, a heat transfer coefficient of  $30 \text{ W}/(\text{m}^2 \cdot \text{K})$  was assumed for the air side. The insulation material used in the test facility was the ultra-flexible foam rubber with a porous foam structure. The conductivity of this material is  $0.036 \text{ W}/(\text{m} \cdot \text{K})$  according to a report for the heat conduction experiment [36]. Calculation parameters and assumptions used are listed in Table 4-3.

**Table 4-3: Parameters and Assumptions used in Energy Evaluation**

<b>Parameters and Assumptions</b>	<b>Unit</b>	<b>Value</b>
D <sub>1</sub> (Inner tube diameter)	mm	4.83
D <sub>2</sub> (Outer tube diameter)	mm	6.35
D <sub>3</sub> (Outer insulation diameter)	mm	25.40
Conductivity of Insulation Material	W/(m·K)	0.036
Air-side Heat Transfer Coefficient	W/(m <sup>2</sup> ·K)	30

Calculated heat gain results are shown in Table 4-4. With all the equations and information stated above, the estimated heat gain from the environment was 14.1 W. After adding this heat gain to the heater power, the modified energy balance for the

evaporator was decreased to 7%. Considering that the mass flow rate was quite small with a relatively large uncertainty on this energy estimation, this number is acceptable.

**Table 4-4: Summary of Heat Gain Calculation**

<b>Variables</b>	<b>Unit</b>	<b>Value</b>
Refrigerant Re Number	-	641.67
Refrigerant Nu Number	-	3.66
Refrigerant-side Heat Transfer Coefficient	W/(m <sup>2</sup> ·K)	67.6
Overall Heat Transfer Coefficient	W/(m <sup>2</sup> ·K)	1.67
Temperature Difference between Air and Refrigerant	K	53.2
Estimated Heat Gain from Ambient	W	14.1

The analysis of heat gain suggests that in refrigeration application, the heat gain from the environment has much greater impact than air conditioning applications and revealed an importance of evaporator section insulation. After the heat gain estimation, the energy balance of evaporator in designed condition was in a reasonable range. This means that the current test results are reliable enough.

In addition to the energy balance analysis of evaporator itself, the energy balance was also checked in system level. More assumptions were made in the system level energy balance analysis as listed below:

- (1) The exposed compressor surface area was 0.02 m<sup>2</sup> with an air-side heat transfer coefficient of 30 W/(m<sup>2</sup>·K). Assuming the compressor temperature was the same as

refrigerant discharge temperature and the whole compressor was at the same temperature.

- (2) Heat losses from the pipe and the condenser capacity were calculated from refrigeration side. Some surface temperature values were used to find state points of each section and the refrigerant side heat transfer capacity was calculated as:

$$Q_i = \dot{m}(h_{out} - h_{in}) \quad (21)$$

- (3) Estimated heat gain in previous section was also included.

Estimation results of system level energy balance are shown in Table 4-5.

**Table 4-5: System Level Energy Balance Evaluation for Baseline Test**

Variables	Unit	Value
Compressor Power	W	54.4
Evaporator Capacity	W	103.83
Estimated Heat Gain in Evaporator	W	14.1
Condenser Heat	W	136.19
Heat Loss in Compressor	W	20.83
Heat Loss in Pipes	W	7.04
Total Energy Input to System	W	172.35
Total Energy Output from System	W	164.06
Deviation	%	5.1

Although some of the values in Table 4-5 were based on assumptions, it can still provide an idea where the heat was exchanged in the system.

Table 4-6 summarizes the energy balance before and after considering the heat gain. In (-10 °C) evaporating temperature condition, the energy balance of the evaporator was improved from 3.1% to 0.1%. And for (-28 °C) conditions, the energy balance improved from 17.7% to 5.1%. It was seen that the more temperature difference between the evaporating temperature and ambient temperature there is, more necessary it is to consider the heat gain.

**Table 4-6 Energy Balance before and after Heat Gain Correction**

Evaporating Temperature	Before Correction	After Correction
-10 °C	3.2%	0.1%
-28 °C	17.7%	5.1%

### 4.3 Ejector-Expansion Refrigeration Cycle Test Results

Before the system was modified, the shakedown test of EERC was conducted. It was observed that the entrainment ratio was only 8%. This also means that not much vapor was pumped from suction port and this made the ejector outlet quality lower. Majority of cooling was transferred to the heater before the compressor because low ejector outlet quality led to two-phase refrigerant flowing through the vapor line after the flash tank. In these circumstances, the EERC system does not provide any benefits. The system was then modified to have a much compact configuration along the ejector suction line, and to prevent the gravity effect, all pipelines and components in that section were positioned at the same height level.

After the modification, components that caused a large pressure drop were either removed or bypassed. As a result, the entrainment ratio was greatly increased, as well as the system COP. Test under  $-10^{\circ}\text{C}$  and 55 Hz condition was conducted and summarized in Table 4-7. However, the EERC test results shown here do not have an improved COP as compared with the baseline VCC. On the contrary, COP was decreased by 29%. Why is there a decrease of EERC performance? This is the next important discussion of this technology.

As compared with the baseline VCC, the benefit of the EERC is coming from a larger latent heat and a higher compressor suction pressure. In Figure 4-3, P-h diagrams of both baseline VCC and EERC are shown. A red dotted line represents the EERC while a blue solid line represents the baseline VCC. First, for the VCC, before and after the isenthalpic expansion process, refrigerant remains at the same enthalpy. Thus, at the outlet of expansion process, the refrigerant becomes two-phase, having a quality around 0.3. However, for the EERC, the available latent heat range for evaporator starts from state 8. This larger enthalpy change means that the EERC has a higher cooling capacity than the baseline VCC at the same mass flow rate. Second, for the baseline VCC, the compression process is from state 9 to state 2'. In the EERC, the compression process is from state 1 to state 2. The baseline VCC's compression process is on the right side of EERC's, which means that the baseline VCC has a lower compressor efficiency, thus a higher compressor power consumption is required. In summary, the EERC could have a higher evaporator capacity and lower compressor work than those of baseline VCC. These are two reasons that the EERC has a theoretically higher COP than the baseline VCC.

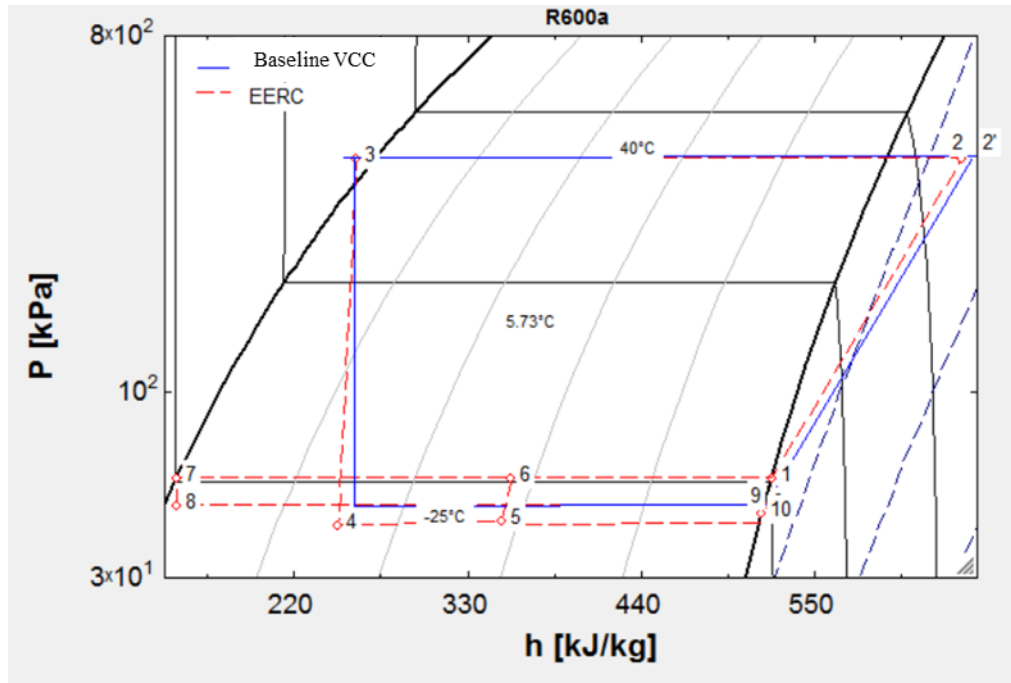


**Figure 4-3: P-h Diagrams of Baseline VCC and EERC**

With the evaporator heater power consumption and ejector suction state, it was found that the refrigerant was in two-phase at the inlet of expansion valve with a quality around 0.15. Theoretically, after the flash tank, only liquid passes through an expansion valve. However, in the test case, the two-phase refrigerant might pass through the expansion valve due to the poor separation of vapor and liquid in the separator. This greatly impaired the expansion process and the evaporator inlet did not reach the minimum latent heat point (shown as state 8 in Figure 4-3).

**Table 4-7: Summary of EERC Test Results at -10°C Evaporating Temperature**

<b>Variables</b>	<b>Unit</b>	<b>EERC Result</b>	<b>Systematic Uncertainty</b>	<b>Random Uncertainty</b>	<b>Total Uncertainty</b>
Compressor Discharge Pressure	kPa	506.7	0.34	2.56	2.90
Condenser Outlet Pressure	kPa	498.8	0.34	0.35	0.69
Ejector Motive Flow Pressure	kPa	495.8	0.34	0.31	0.65
Ejector Suction Pressure	kPa	99.4	0.34	1.18	1.52
Flash Tank Pressure	kPa	99.9	0.34	1.20	1.54
Compressor Suction Pressure	kPa	98.9	0.34	1.28	1.62
Compressor Discharge Temperature	°C	55.5	0.5	0.09	0.59
Condenser Outlet Temperature	°C	26.4	0.5	0.03	0.53
Ejector Motive Flow Temperature	°C	24.6	0.5	0.04	0.54
Ejector Suction Temperature	°C	-8.5	0.5	0.45	0.95
Evaporating Temperature	°C	-10.4	0.5	0.25	0.75
Compressor Suction Temperature	°C	23.5	0.5	1.32	1.82
Room Temperature	°C	26.0	0.5	0.10	0.6
Motive Flow Mass Flow Rate	g/s	0.87	0.003	0.002	0.005
Suction Flow Mass Flow Rate	g/s	0.35	0.001	0.003	0.004
Entrainment Ratio	-	0.40	0.002	0.004	0.006
Compressor Power Consumption	W	92.1	0.27	0.42	0.69
Low Temp Evap. Capacity	W	106.6	0.21	2.68	2.89
High Temp Evap. Capacity	W	97.3	0.21	1.01	1.22
Cooling COP	-	2.2	0.007	0.033	0.04

**Table 4-8: Comparison of Test Results between VCC and EERC**

Variables	Unit	VCC	Total		Total
			Uncertainty		
Compressor Discharge Pressure	kPa	499.3	2.90	506.7	2.90
Condenser Outlet Pressure	kPa	488.5	0.83	498.8	0.69
Ejector Motive Flow Pressure	kPa			495.8	0.65
Ejector Suction Flow Pressure	kPa			<b>99.4</b>	1.52
Flash Tank Pressure	kPa			<b>99.9</b>	1.54
Compressor Suction Pressure	kPa	98.6	0.61	98.9	1.62
Compressor Discharge Temperature	°C	53.9	0.59	55.5	0.59
Condenser Outlet Temperature	°C	25.1	0.56	26.4	0.53
Ejector Motive Flow Temperature	°C			24.6	0.54
Ejector Suction Flow Temperature	°C			-8.5	0.95
Evaporating Temperature	°C	-10.2	0.58	-10.4	0.75
Compressor Suction Temperature	°C	22.7	0.58	23.5	1.82
Room Temperature	°C	24.7	0.60	26.0	0.6
Motive Flow Mass Flow Rate	g/s	0.88	0.007	0.87	0.005
Suction Flow Mass Flow Rate	g/s			0.35	0.004
Entrainment Ratio	-			<b>0.40</b>	0.006
Compressor Power Consumption	W	91.1	0.63	92.1	0.69
Low Temp Evap. Capacity	W	284.4	1.30	106.6	2.89
High Temp Evap. Capacity	W			97.3	1.22
Cooling COP	-	<b>3.1</b>	0.04	<b>2.2</b>	0.04

Based on Table 4-8, it was observed that when the ejector suction pressure and flash tank pressure were compared, the diffuser pressure lift observed was only 0.5 kPa, which is close to the range of uncertainty. Furthermore, when the ejector suction pressure and compressor suction pressure were compared, the compressor suction pressure was even 0.5 kPa lower than the ejector suction pressure.

Whereas it was found that the pressure inside the diffuser showed a higher pressure than the flash tank. Then there was a sudden expansion and a sudden contraction of the flow in flash tank, which caused a pressure drop. Pressure losses by sudden expansion and contraction were then evaluated in EES, and the results are summarized in Table 4-9. After considering the pressure drop associated with sudden expansion and sudden contraction, the real ejector exit pressure in the test should be 101.7 kPa. Therefore, a pressure lift of 2.3 kPa was reached in the test. However, this lift is much lower than expected.

In summary, the EERC test results show a narrower latent heat range for evaporator and a negligible pressure lift of ejector. Thus, the two benefits of EERC were not achieved and resulted in a lower COP than the baseline VCC.

**Table 4-9: Evaluation of Sudden Expansion and Sudden Contraction**

<b>Variables</b>	<b>Unit</b>	<b>Value</b>
Flash Tank Pressure	kPa	99.9
Flash Tank Liquid Pressure	kPa	101.3
Motive Flow Mass Flow Rate	g/s	0.87
Suction Flow Mass Flow Rate	g/s	0.35
Ejector Exit Pressure	kPa	101.7

Although the test results did not meet the expectation, it also gave us chance to analyze the reason for this outcome, which is important for the development of future improved EERC technology. As discussed, it is necessary to identify how to improve the pressure lift of ejector and how to achieve a better separation of vapor and liquid.

Important factors of ejector performance are ejector efficiencies in different sections. These efficiencies define how close the really process in ejector is as compared with an isentropic process. The designed efficiencies under test conditions were 0.8, 0.9, 0.7, and 0.7 for motive nozzle efficiency, suction nozzle efficiency, mixing efficiency and diffuser efficiency, respectively. The ejector was modeled as a single component in the EES to explore what the pressure lift of the ejector should be when the ejector dimensions were used in the modeling. Results are summarized in Table 4-10. Four calculated values, including motive nozzle exit quality, mixing velocity, ejector exit pressure and velocity, are listed in the lower section of the table. It can be seen that with the designed efficiencies, a pressure lift of 5.6 kPa can be achieved with current ejector prototype. Therefore, there is still a gap of 3.3 kPa between the test and designed condition. One of

the reason could be that the pressure recovery inside the diffuser did not meet the design condition. Therefore, the two-phase refrigerant might still carry a large kinetic energy at the exit of ejector. When this high velocity flow enters the flash tank, the pressure loss by sudden expansion is even higher, and this loss diminishes the recovery work from the ejector.

**Table 4-10: Pressure Lift Estimation under Designed Efficiencies**

<b>Variables</b>	<b>Unit</b>	<b>Value</b>
Ejector Motive Flow Pressure	kPa	495.8
Ejector Motive Flow Temperature	°C	24.6
Motive Flow Mass Flow Rate	g/s	0.87
Ejector Suction Pressure	kPa	99.4
Ejector Suction Temperature	°C	-8.5
Suction Flow Mass Flow Rate	g/s	0.35
Mixing Pressure	kPa	99.4
Motive Nozzle Exit Velocity	m/s	100.2
Mixing Velocity	m/s	50.72
Estimated Ejector Exit Pressure	kPa	105
Ejector Exit Quality	-	0.45

For the control aspect of EERC, the entrainment ratio and pressure lift affect each other by the opening of expansion valve. For the same geometry ejector, high pressure lift could be achieved but entrainment ratio would be decreased when the expansion valve

opening is reduced. On the other hand, entrainment ratio would be increased to have more cooling capacity but pressure lift effect of ejector could be reduced when the expansion valve opening is enlarged. Therefore, theoretically there is an optimized opening under each operating condition.

It is obvious that the suction flow rate would increase too with the motive flow.

Therefore, it is worth to see whether changing the compressor frequency would have some improvement on the entrainment ratio. With higher compressor frequency, the motive flow rate increases while it consumes more compressor power.

In total, four compressor frequency conditions were tested at 55, 65, 75, and 85 Hz. The evaporating temperature was kept the same for all four conditions. The COPs under different compressor frequencies are shown in Figure 4-4. A small increase trend in COP is shown with the compressor frequency. However, the increase rate is not large enough to reduce the COP difference between the baseline VCC and EERC.

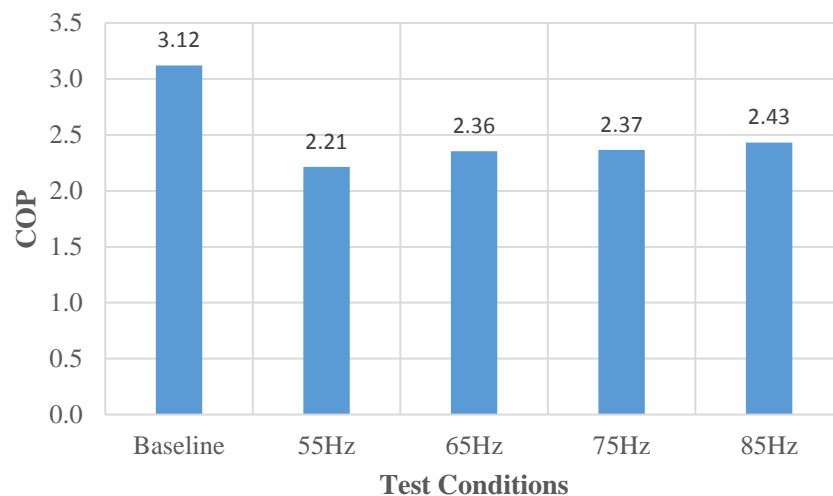


**Figure 4-4: System COP under Different Compressor Frequencies**

Figure 4-5 shows the trend of mass flow rates and entrainment ratio with compressor frequency variation. It is observed that in general, both motive flow rate and suction flow rate increase with compressor frequency. However, as for the entrainment ratio, there was a peak appeared at the frequency of 75 Hz. This frequency could be an optimum operating condition for the given ejector.

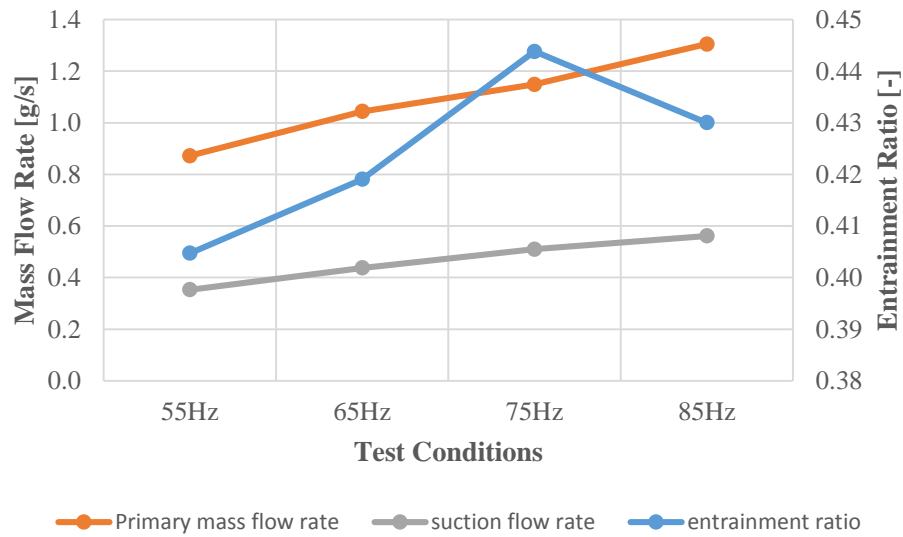


**Figure 4-5: Flow Rates and Entrainment Ratio under Different Compressor Frequencies**

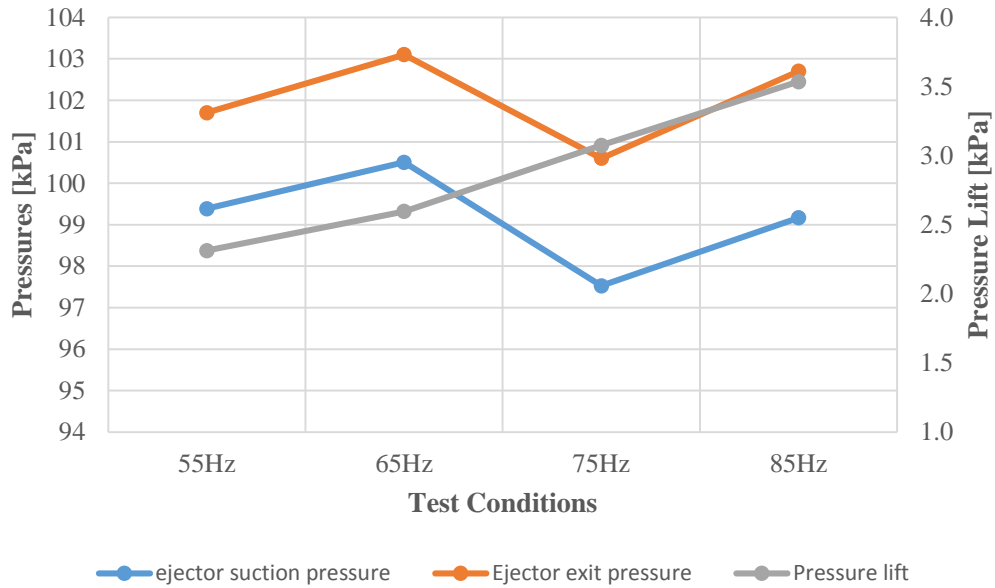


**Figure 4-6: Ejector Pressure Lift under Different Compressor Frequencies**

Figure 4-6 provides the trend of pressure lift of ejector under different working conditions. One thing to be noted here is that this pressure lift is the pressure difference between flash tank pressure and ejector suction pressure. It was observed with increase of compressor frequency, the pressure lift also increased but in a small scale.

With the discussion of compressor frequency, it can be concluded that the increase of compressor frequency can lead to a higher entrainment ratio and higher pressure lift.

However, this increase effect is limited.

#### 4.4 Summary of Experimental Results

The baseline VCC and EERC were tested under  $-10^{\circ}\text{C}$  evaporating temperature. Effects of different compressor frequency were evaluated. The designed ejector prototype did not performed well enough to meet the target performance and further study is needed for further improvement.

The inferior performance of current EERC system is reasoned as follows:

- Poor mixing inside ejector leads to less pressure recovery in the diffuser.
- Poor pressure recovery in the diffuser leads to poor liquid-vapor separation.
- Two-phase refrigerant entering the suction line impaired the control of expansion valve and also results in a less evaporator capacity.
- The failure of expansion valve control affects the ejector suction pressure, which also affects the mixing inside the ejector.

To improve the performance of current EERC system, the mixing condition inside this ejector prototype should be studied. Once the mixing of two flows becomes better, all the components would have a better performance. This also means that in the application of EERC, the mixing condition inside the ejector is very critical.

During the study of EERC system operating at sub-zero evaporating temperature, several important observations were made for a better performance of the system:

- Pressure drop along the ejector suction loop has an important effect on the entrainment ratio. It is necessary to have low-pressure-drop evaporator in the system.
- Since the evaporating temperature is below 0°C, and the ejector, the flash tank, and every component in the ejector suction loop would remain at this low temperature. Therefore, it is very important to have a good thermal insulation for these components and prevent any heat gain except the evaporator.
- In the application of domestic refrigerator, the flow rate of the refrigerant is very small, so that the transient effect of the system is very different. To prevent the

unexpected migration of the refrigerant, a receiver should be carefully sized while considering the flash tank volume.

- System should be designed to prevent oil trapping in the ejector suction loop.

## **5. Thermodynamic Modeling of Ejector-Expansion Refrigeration Cycle**

Test results shown in Chapter 4 indicate that a better design is needed for the EERC at low evaporating temperature. To ensure a reliable design, thermodynamic model was developed for EERC to have a more accurate prediction of the system performance. The model was validated using the data in Table 4-7. In overall, the thermodynamic model had a fair prediction of the system performance and can be used for future design.

### **5.1 Cycle Modeling**

To better understand how the EERC works, the thermodynamic model of the whole system was developed using the EES. The design geometries of the ejector were used in the model to find relations between refrigerant states and velocities inside the ejector. The parameters and the efficiency correlation of the variable speed compressor were used to calculate the power consumption and motive flow rate in the system. The goal of the EERC thermodynamic model development was to calculate the flow rate range and simulate the expected EERC COP at all possible operating conditions. Therefore, several assumptions were necessary for the compressor suction pressure and ejector motive nozzle exit pressure. These two assumptions would set the ejector operating conditions in the EERC model. First, the model was run under one certain set of assumptions to see what the expected system performance would be. Then more parametric study was conducted while changing these assumptions.

In the simulation,  $-10^{\circ}\text{C}$  evaporating temperature condition was used to keep a same working condition. The two specific assumptions used are: (1) compressor suction pressure at 115 kPa and (2) ejector motive nozzle exit pressure at 102 kPa. Other additional assumptions to simplify the problem include: (1) no pressure drop considered

at heat exchangers, flash tank and pipes, (2) system is under thermodynamic steady state, and (3) ejector performance can be predicted under 1-D thermodynamic model.

## **5.2 Modeling Results**

Under the assumptions and conditions stated in previous section, the EERC was modeled under the  $-10^{\circ}\text{C}$  evaporating temperature and 65 Hz compressor frequency. Results are shown in Table 5-1. From the simulation result, it was observed that the high side pressure of the system reached around 500 kPa, while the evaporator kept a pressure at 108.1 kPa. With the compressor running at 65 Hz frequency, the expected power consumption could reach to 102.7 W. The motive flow rate in the simulation was determined by the compressor model at given inlet refrigerant density. The suction flow of the ejector was determined by suction density, and mostly by the pressure at motive nozzle exit. Simulation results show that an entrainment ratio of 0.75 and a total COP of 3.7 could be achieved in this condition.

In order to investigate the effects of assumption variations, the parametric study was conducted with some physical boundary conditions. Since the evaporating pressure was 108.1 kPa, the motive nozzle exit pressure could not be higher than this value. Therefore, in the parametric study, the ejector nozzle exit pressure was varied from 90 to 108 kPa. Then for the compressor suction pressure, it was assumed that it was 0 to 40 kPa higher than the evaporating pressure. The parametric study results with these boundary conditions are shown in Figure 5-1 and Figure 5-2.

**Table 5-1: Simulation Results of EERC under -10°C Evaporating Temperature**

<b>Variables</b>	<b>Unit</b>	<b>EERC Result</b>
Compressor Discharge Pressure	kPa	503.5
Ejector Motive Flow Pressure	kPa	503.5
Ejector Suction Pressure	kPa	108.1
Mixing Pressure	kPa	102
Compressor Suction Pressure	kPa	115
Compressor Discharge Temperature	°C	71.1
Ejector Motive Flow Temperature	°C	28
Ejector Suction Temperature	°C	-10
Compressor Suction Temperature	°C	21.6
Motive Flow Mass Flow Rate	g/s	1.19
Suction Mass Flow Rate	g/s	0.89
Ejector Exit Quality	-	0.57
Compressor Frequency	Hz	55
Compressor Power Consumption	W	102.7
Low Temp Evap. Capacity	W	322.2
High Temp Evap. Capacity	W	58.2
Entrainment Ratio	-	0.75
Cooling COP	-	3.7

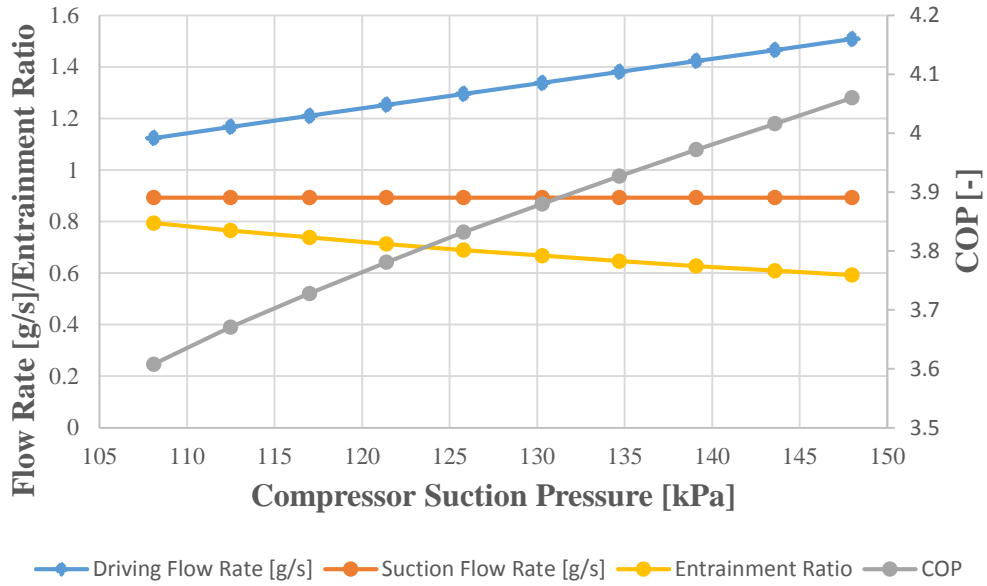


**Figure 5-1: Parametric Study of Compressor Suction Pressure**

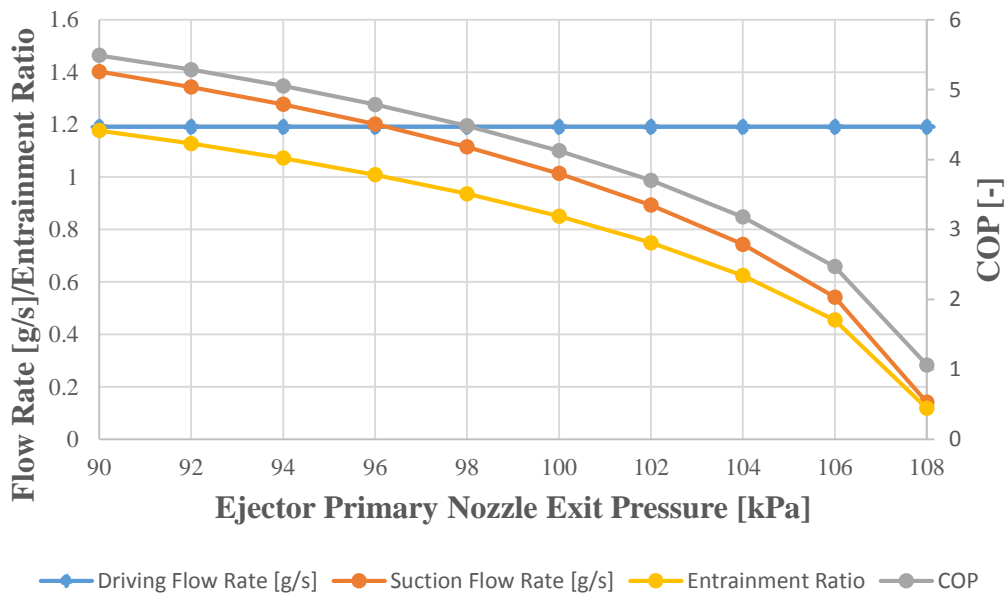


**Figure 5-2: Parametric Study of Ejector Nozzle Exit Pressure**

In the parametric study of compressor suction pressure, the ejector motive nozzle exit pressure was set at 102 kPa. In the result, it can be seen that the change of compressor suction pressure would not affect the suction flow rate because the suction flow rate was

largely determined by the ejector motive nozzle exit pressure. However, the change of compressor suction pressure affected the motive flow rate, thus a decrease of entrainment ratio was observed in the Figure 5-1. One interesting thing to be noted here is that the overall COP of the system is not decreased although the entrainment ratio is decreased. The increase of pressure lift of the ejector is as important as an increase of compressor suction pressure. From this prospective, the COP of EERC system does not simply depend on the entrainment ratio, but also depends on the pressure lift of the ejector, or some other factors.

Similarly, a second parametric study about ejector motive nozzle exit pressure was conducted for an ejector motive nozzle exit pressure. In this case, the motive flow rate kept the same because the compressor suction flow rate was not changing. However, the suction flow rate, entrainment ratio and COP were decreased in a large degree. When the ejector motive nozzle exit pressure was very close to the evaporating pressure, the suction flow rate could be reduced to 0. Both entrainment ratio and system COP would be greatly affected by this change.

Based on the results of these two parametric studies, it was concluded that the system performance is more sensitive to the ejector motive nozzle design. When the pressure at motive nozzle exit is not low enough, the pumping effect of ejector can be largely impaired. This can also be used in the following analysis of the EERC system.

### **5.3 Model Validation**

It is necessary to see whether the model developed in Chapter 4 agrees with the test results and whether we can use the model to predict the performance under various conditions. First, one validation was conducted for  $-10^{\circ}\text{C}$  evaporating temperature

condition with 55 Hz frequency. The way to validate was utilizing pressure and temperature measured for each state point as inputs. By calculating the thermodynamic properties of all state points, the mass flow rate, compressor power consumption, and heater capacities were validated. Table 5-2 compares the results calculated by the model and the test under the -10°C evaporating temperature and 55 Hz compressor frequency.

**Table 5-2: Comparison of Model Results and Test Results**

<b>Variables</b>	<b>Unit</b>	<b>Model Results</b>	<b>Test Results</b>	<b>Deviation</b>
Motive Flow Mass Flow Rate	g/s	0.86	0.87	0.01
Suction Flow Mass Flow Rate	g/s	0.30	0.35	0.14
Compressor Power	W	93.8	92.1	0.02
Low Temp Evap. Capacity	W	109.9	106.6	0.03
High Temp Evap. Capacity	W	49.6	97.3	0.49
COP	-	1.7	2.2	0.23

Overall, the model has a good prediction for compressor power consumption, motive flow mass flow rate and evaporator capacity within 3% accuracy. The motive flow mass flow rate and the compressor power consumption could be predicted by the compressor model developed with the compressor working pressure ratio set by the inputs. The fact that the model predicted values well matched with the measured values indicates that the compressor model has a good performance prediction. However, the model prediction has a relatively large deviation from the test results for suction mass flow rate and the heater input before the compressor. This was because there was a poor mixing inside the ejector and the separation of the flash tank was not well done so that the refrigerant sent to the vapor line and liquid line were both in two-phase. With the limited information, it

was impossible to know the exact quality at the flash tank exit. Therefore, the model predictions for the suction flow rate and the heater capacity before the compressor were not good enough.

As discussed in the section 5.3, when two-phase flow came out of the flash tank's vapor line, the cooling capacity of the low temperature evaporator would transfer to the high temperature evaporator. Therefore, the predicted capacity of high temperature evaporator would be lower than the test result. The COP results of modeling and test are both calculated using the definition in Eq. (4). Capacities of high temperature evaporator and low temperature evaporator were added together to represent the total cooling capacity of the system. Although the system model had a good prediction for the low temperature evaporator capacity, the predicted high temperature evaporator capacity was lower than the test results. The reason for this is that two-phase refrigerant entering the high temperature evaporator resulted in a phase change in the high temperature evaporator, which transferred a latent heat capacity to the high temperature evaporator.

When both modeling results and test results are shown on P-h diagram, as Figure 5-3, it is more obvious to see the reason for low COP in the test. One thing to be noted here is that in the test two-phase was observed to enter the low temperature evaporator and high temperature evaporator but the quality of the two-phase cannot be known, so in the test results of Figure 5-3, it is still assumed to have a good separation in the flash tank.

In Figure 5-3, a small pressure lift of test results is shown between state 5' and state 6', which represents the pressure lift of the ejector, however, the pressure lift was limited compared to the designed modeling results. There are two reasons for this limited

pressure lift of the ejector: one is because of the poor mixing and not complete pressure recovery inside the ejector; the other reason is because poor separation inside the flash tank leads to two-phase entering the expansion valve, however, two-phase flow largely impairs the performance of expansion valve control, no pressure difference was built before and after the expansion valve.

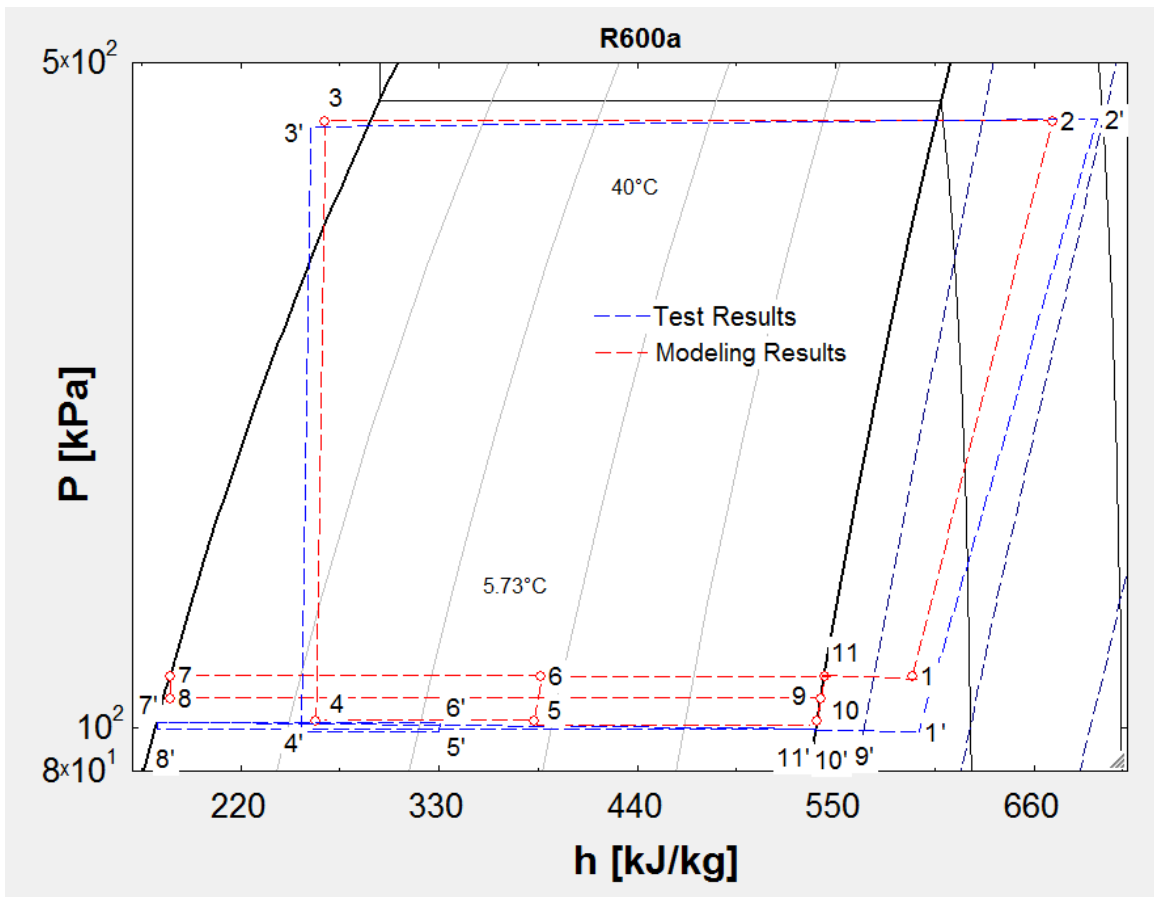
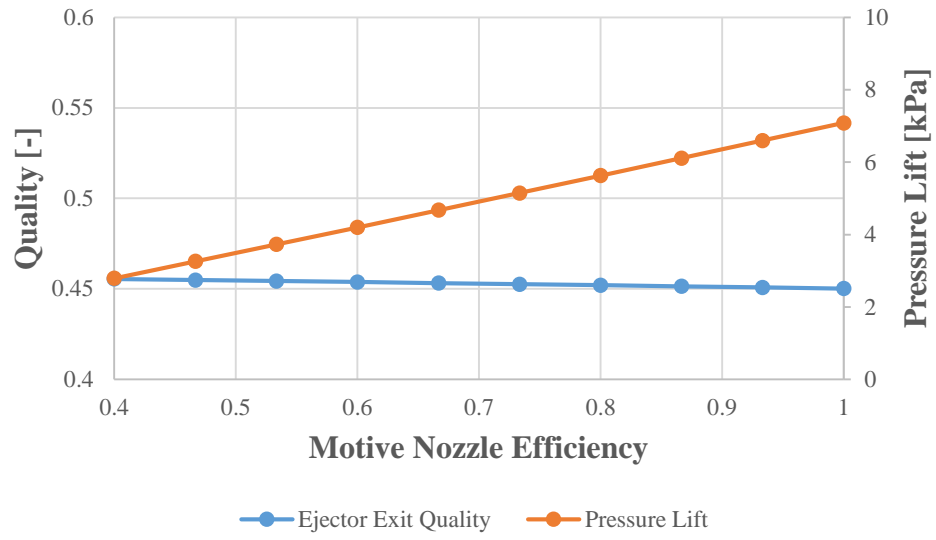


**Figure 5-3 Comparison of P-h diagram between Modeling Results and Test Results**  
 Moreover, in the test results, pressure drop in the heat exchangers are included, which results in an even lower compressor suction pressure. In summary, it is because of limit pressure lift that results in a not match performance between modeling results and test results.

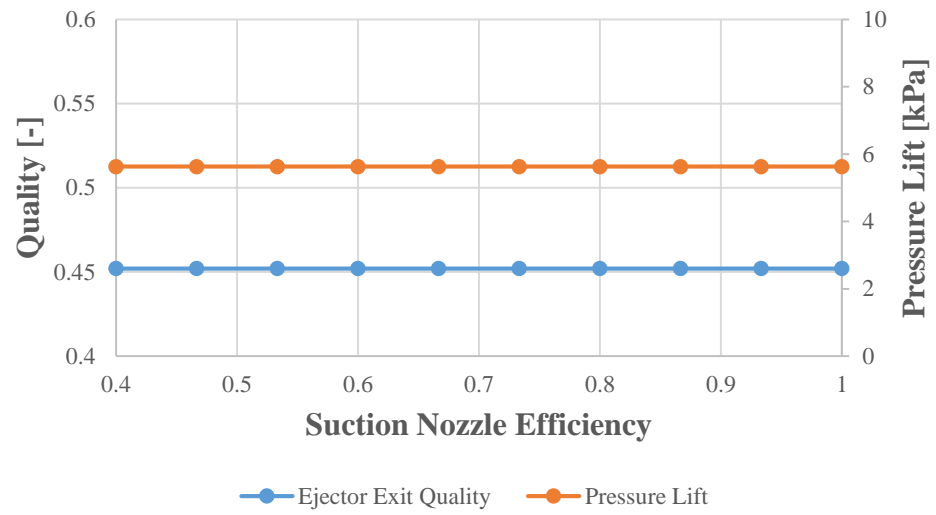
## 5.4 Discussion

Based on the analysis in Chapter 5, the diffuser pressure lift largely depends on the ejector efficiencies. As the most important factors in ejector operation, the efficiencies of each part can have different sensitivity to the overall ejector performance. Therefore, the sensitivity study would be of great help for future improved design. In the sensitivity study, all of the efficiencies varied from 0.4 to 1.0. When one efficiency was varied, all the other efficiencies kept the same as the designed efficiency.

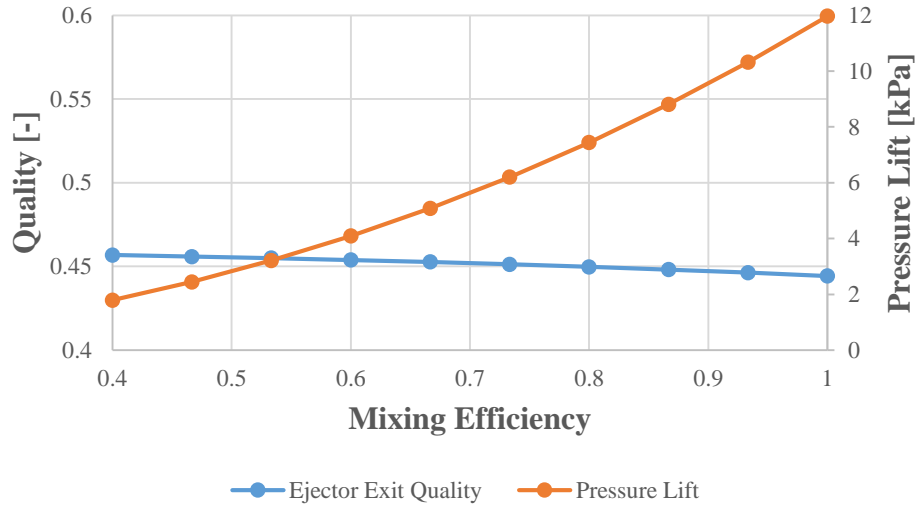
Figure 5-4 shows the sensitivity study results when each of the efficiency varied. The scales for the exit quality and pressure lift were adjusted to the same except for the mixing efficiency. From the figure, it was observed that the mixing efficiency has the largest effect on both pressure lift and exit quality. The effect of motive nozzle and diffuser efficiencies were similar to each other while the suction nozzle efficiency showed the least sensitivity to the ejector performance. These results provide the idea that if the mixing condition inside the ejector was poor, both entrainment ratio and pressure lift would be largely affected.



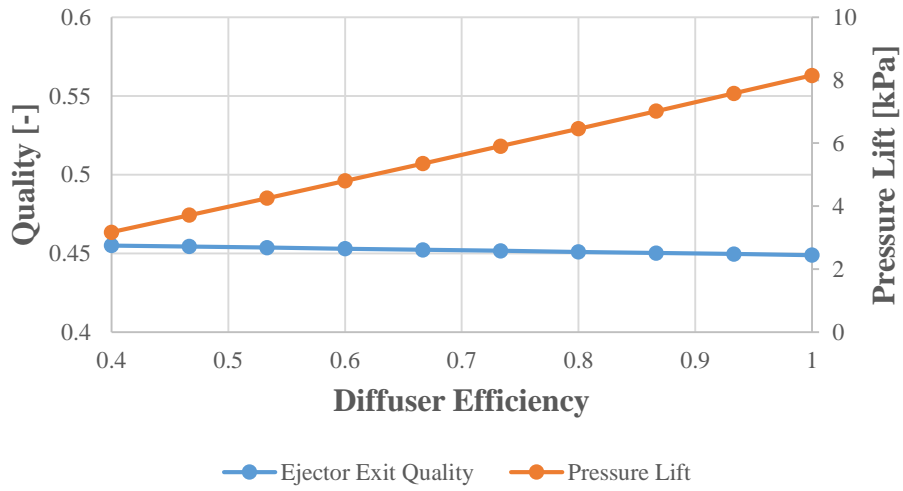
(a)



(b)



(c)



(d)

**Figure 5-4: Sensitivity Study of Ejector Efficiencies**

## 6. Conclusions

In this study, the ejector prototype designed for a domestic refrigerator was fabricated based on its design optimization from the previous research. The test facility was developed to evaluate the EERC with R600a (isobutane). Tests of VCC were conducted first under  $-10^{\circ}\text{C}$  and  $-28^{\circ}\text{C}$  evaporating temperatures. Then, the EERC system was tested and analyzed under the  $-10^{\circ}\text{C}$  condition. For the further investigation, the thermodynamic model of the EERC system was developed. The conclusions of the study are summarized as follows:

- For the baseline test, when the evaporating temperature was  $-10^{\circ}\text{C}$ , the mass flow rate was  $0.88\text{ g/s}$  and COP was 3.1. When the evaporating temperature was decreased to  $-28^{\circ}\text{C}$ , COP decreased to 1.9.
- The prototype EERC system achieved COP at 2.2 to 2.4 under the  $-10^{\circ}\text{C}$  evaporating temperature condition.
- The EERC system was modeled to predict its performance. When the compressor suction pressure was 115 kPa and the ejector motive nozzle exit pressure was 102 kPa, the entrainment ratio and COP were calculated to be 0.75 and 3.7, respectively.
- Furthermore, parametric studies of the compressor suction pressure and the ejector motive nozzle exit pressure were conducted. It was concluded that the ejector motive nozzle exit pressure has the most significant effect on the system performance.
- It was also concluded that poor mixing inside ejector led to a lower pressure lift and an impaired performance of EERC system.
- Effect of the compressor frequency on the EERC system was also studied experimentally. Four tests were conducted under 55, 65, 75 and 85 Hz compressor

frequencies. A small increase trend of the COP and pressure lift was observed.

However, the increase was limited.

- Worthy experiences were gained for future study of this technology, including the selection of components and construction of refrigerant pipeline. One important lesson was to keep the pressure drop in the ejector suction loop low enough to have a desired suction effect.

## 7. Future Work

To better understand and improve the system performance of the existing system, several future works are suggested as follows:

- **Mixing efficiency:** Since it was proven that the mixing efficiency of the ejector has a significant effect on the system performance, the mixing condition inside the ejector needs to be studied more. Considering the difficulty of getting instantaneous information of flow inside ejector, the flow visualization of flow mixing inside the ejector can be a feasible approach to have an idea of improving the mixing performance.
- **Flash tank:** The effect of separation efficiency of the liquid vapor separator and the method for its proper sizing are needed to investigate.
- **Refrigerant migration:** It was observed in the test that there was a refrigerant migration during the startup and shut down processes of the system. Unexpected migration may influence the next startup of the system. Therefore, the transient effect of EERC system should be investigated.
- **Control:** During the test, the proper control of the whole EERC system was much more complicated than the baseline VCC. Therefore, the control strategy of EERC system should be studied to reach a steady state condition easier and faster.

## Reference

- [1] Lawrence Livermore National Laboratory, related news: U.S. Coal Use Up, Says Energy Department.
- [2] BP, Statistical Review of World Energy, 2013.
- [3] U.S. Energy Information Administration, Residential Energy Consumption Survey, 2009.
- [4] U.S. Energy Information Administration, Commercial Buildings Energy Consumption Survey, 2003.
- [5] R. Yapici, H.K. Ersoy, *Performance characteristics of the ejector refrigeration system based on the constant area ejector flow model*, Energy Conversion and Management, 2005. 46(18-19): pp.3117-3135
- [6] K. Sumeru, *A review on two-phase ejector as an expansion device in vapor compression refrigeration cycle*, Renewable Sustainable Energy Review, 2012. 16(7): pp. 4927-4937
- [7] J.H. Keenan, E.P. Neumann, F. Lustwerk, *An investigation of ejector design by analysis and experiment*. 1950, pp.299-309
- [8] B.J. Huang, *A 1-D analysis of ejector performance*, International Journal of Refrigeration, 1999. 22(5): pp.352-364
- [9] Sun, D.W, Eames IW. *Recent developments in the design theories and applications of ejectors—a review*, Journal of Institute Energy 1995. 68(475): pp.65–79.

- [10] S.A. Sherif, *Analysis and modeling of a two-phase jet pump of a thermal management system for aerospace applications*, International Journal of Mechanical Sciences, 2000. 42(2): pp.185-198
- [11] S. He, *Progress of mathematical modeling on ejectors*, Renewable and Sustainable Energy Reviews, 2009. 13(8): pp.1760-1780
- [12] T. Sriveerakul, *Performance prediction of steam ejector using computational fluid dynamics: Part 1. Validation of the CFD results*, International Journal of Thermal Sciences, 2007. 46(8): pp.812-822
- [13] T. Sriveerakul, *Performance prediction of steam ejector using computational fluid dynamics: Part 2. Flow structure of a steam ejector influenced by operating pressures and geometries*, International Journal of Thermal Sciences, 2007. 46(8): pp.823-833
- [14] Y. Bartosiewicz, *Numerical assessment of ejector operation for refrigeration applications based on CFD*, Applied thermal engineering, 2006. 26(5-6): pp.604-612
- [15] A.A. Kornhauser, *The Use of an Ejector as a Refrigerant Expander*, International Refrigeration and Air Conditioning Conference, 1990.
- [16] E. Nehdi, *Performance analysis of the vapor compression cycle using ejector as an expander*, International Journal of Energy Research, 2006. 31(4): pp.364-375
- [17] N. Bilir, *Performance improvement of the vapor compression refrigeration cycle by a two-phase constant area ejector*, International Journal of Energy Research, 2008. 33(5): pp.469-480

- [18] J. Sarkar, *Geometric parameter optimization of ejector-expansion refrigeration cycle with natural refrigerants*, International Journal of Energy Research, 2010. 34(1): pp.84-94
- [19] G.S. Harrell, *Performance tests of a two-phase ejector*, Proceedings of the 30th Intersociety Energy Conversion Engineering Conference, 1995.
- [20] P. Menegay, *Improvements to the ejector expansion refrigeration cycle*, 31th Intersociety Energy Conversion Engineering Conference, 1996.
- [21] G. Pottker, *Experimental investigation of an R410A vapor compression system working with an ejector*, International refrigeration and air conditioning conference, Purdue University, 2010.
- [22] S. Disawas, *Experimental investigation on the performance of the refrigeration cycle using a two-phase ejector as an expansion device*, International Journal of Refrigeration, 2004. 27(6): pp.587-594
- [23] J.P. Liu, J.P. Chen, Z.J. Chen, *Thermodynamic analysis on trans-critical R744 vapor compression/ejection hybrid refrigeration cycle*, Proceedings of fifth IIR G. Lorentzen conference on natural working fluids, 2002.
- [24] Li, Groll, *Transcritical CO<sub>2</sub> refrigeration cycle with ejector-expansion device*, International Journal of Refrigeration, 2005. 28(5): pp.766-773
- [25] S.W. Elbel, P.S. Hrnjak, *Effect of internal heat exchanger on performance of transcritical CO<sub>2</sub> systems with ejector*, Tenth international refrigeration and air conditioning conference at Purdue.

- [26] M. Nakagawa, *Experimental investigation on the effect of mixing length on the performance of two-phase ejector for CO<sub>2</sub> refrigeration cycle with and without heat exchanger*, International Journal of Refrigeration, 2011. 34(7): pp.1604-1613
- [27] L. Kairouani, *Use of ejectors in a multi-evaporator refrigeration system for performance enhancement*, International Journal of Refrigeration, 2009. 32(6): pp.1173-1185
- [28] Yicai Liu, *Compression-injection hybrid refrigeration cycles in household refrigerators*, Applied Thermal Engineering, 2010. 30(16): pp.2442-2447
- [29] Tao Bai, *Thermodynamics analysis of a modified dual-evaporator CO<sub>2</sub> transcritical refrigeration cycle with two-stage ejector*, Energy, 2015. 84(1): pp.325-335
- [30] Lin Zhu, *Performance analysis of a novel dual-nozzle ejector enhanced cycle for solar assisted air-source heat pump systems*, Renewable Energy, 2014. 63: pp.735-740
- [31] U.S. Environmental Protection Agency, *Transitioning to Low-GWP Alternatives in Commercial Refrigeration*, 2010.
- [32] Ioan Sarbu, *A review on substitution strategy of non-ecological refrigerants from vapour compression-based refrigeration, air-conditioning and heat pump systems*, International Journal of Refrigeration, 2014. 46: pp.123-141
- [33] M.N.V. Naduvath, *Investigation of Single and Two-Phase Flow Ejectors*, PhD Dissertation, University of Maryland, 1999.
- [34] Parker O-ring Handbook, ORD 5700, 2007
- [35] Electric Expansion Valves, SER, SERI, SEHI manual, Sporlan, Parker.

[36] Alan Guthrie, Michael Hartley, Alex Moon, and Krista Simonson, Redesigning the ME 331 Heat Conduction Experiment, Report, 2012